

**Fig. 4.** Multiyear predictions of AMOC transport. RAPID/MOCHA time series are shown in red; ensemble mean forecasts are shown in dark gray, light blue, dark blue, and green for the forecasts starting in January 2008, January 2009, January 2010, and January 2011, respectively. The pale shading represents the 95% confidence intervals of the nine-member forecast ensemble initialized in January 2008, January 2009, January 2010, and January 2011.

not—is inevitable for as long as in situ ocean interior measurements cannot be made in real time.

For all start years, the ensemble-mean forecasts until 2014 indicate a generally stable AMOC (Fig. 4). However, the forecast initialized in 2010 shows a pronounced AMOC minimum in March 2010 that arises from a minimum in EK (fig. S7).

which in turn is induced by an extremely negative North Atlantic Oscillation in winter 2009–2010 (28). The real AMOC minimum in March 2010 may turn out to be even deeper than predicted, because our ensemble mean underpredicts AMOC amplitude (fig. S2). We are confident, however, that the AMOC minimum in March 2010 will be a short-lived phenomenon; our confidence is based on the insensitivity of our AMOC and MO forecasts to the start year.

We cannot readily generalize our results for 26.5°N to other latitudes; recent studies reported a change in the character of AMOC fluctuations around 40°N, with a strong decadal component to the north and enhanced higher-frequency variability to the south (29–31). However, for 26.5°N, we have established AMOC hindcast skill, we understand that this skill arises from the mid-ocean transport, and we confidently predict a stable AMOC at least until the end of 2014. Moreover, our findings demonstrate that skill in climate prediction arises not only from the large ocean thermal inertia but potentially also from the long time scales of internal ocean dynamics.

#### References and Notes

1. J. R. Knight, R. J. Allan, C. K. Folland, M. Vellinga, M. E. Mann, *Geophys. Res. Lett.* **32**, L20708 (2005).
2. R. T. Sutton, D. L. R. Hodson, *Science* **309**, 115 (2005).
3. H. Pohlmann, F. Sienz, M. Latif, *J. Clim.* **19**, 6062 (2006).
4. J. R. Knight, C. K. Folland, A. A. Scaife, *Geophys. Res. Lett.* **33**, L17706 (2006).
5. R. Zhang, T. Delworth, *Geophys. Res. Lett.* **33**, L17712 (2006).
6. D. Hodson *et al.*, *Clim. Dyn.* **34**, 1041 (2010).
7. D. M. Smith *et al.*, *Science* **317**, 796 (2007).
8. N. S. Keenlyside, M. Latif, J. Jungclaus, L. Kornblueh, E. Roeckner, *Nature* **453**, 84 (2008).
9. H. Pohlmann, J. H. Jungclaus, A. Köhl, D. Stammer, J. Marotzke, *J. Clim.* **22**, 3926 (2009).
10. T. Mochizuki *et al.*, *Proc. Natl. Acad. Sci. U.S.A.* **107**, 1833 (2010).
11. D. M. Smith *et al.*, *Nat. Geosci.* **3**, 846 (2010).
12. H. Pohlmann *et al.*, *J. Clim.* **17**, 4463 (2004).

13. M. Collins *et al.*, *J. Clim.* **19**, 1195 (2006).
14. E. Hawkins, R. Sutton, *Geophys. Res. Lett.* **35**, L11603 (2008).
15. R. Msadek, K. W. Dixon, T. L. Delworth, W. Hurlin, *Geophys. Res. Lett.* **37**, L19608 (2010).
16. S. A. Cunningham *et al.*, *Science* **317**, 935 (2007).
17. T. Kanzow *et al.*, *Science* **317**, 938 (2007).
18. J. H. Jungclaus *et al.*, *J. Clim.* **19**, 3952 (2006).
19. C. M. Domingues *et al.*, *Nature* **453**, 1090 (2008).
20. D. Stammer, WCRP Informal Publication No. 9, *ICPO Publication Series 93* (International CLIVAR Project Office, Southampton, UK, 2006).
21. E. Munoz, B. Kirtman, W. Weijer, *Deep Sea Res. Part II Top. Stud. Oceanogr.* **58**, 1848 (2011).
22. E. Kalnay *et al.*, *Bull. Am. Meteorol. Soc.* **77**, 437 (1996).
23. Materials and methods are available as supporting material on *Science Online*.
24. S. M. Olsen, B. Hansen, D. Quadfasel, S. Østerhus, *Nature* **455**, 519 (2008).
25. T. Kanzow *et al.*, *J. Clim.* **23**, 5678 (2010).
26. M. P. Chidichimo, T. Kanzow, S. A. Cunningham, W. E. Johns, J. Marotzke, *Ocean Sci.* **6**, 475 (2010).
27. J. Hirschi *et al.*, *Geophys. Res. Lett.* **30**, 1413 (2003).
28. T. Jung, F. Vitart, L. Ferranti, J.-J. Morcrette, *Geophys. Res. Lett.* **38**, L07701 (2011).
29. R. J. Bingham, C. W. Hughes, V. Roussenov, R. G. Williams, *Geophys. Res. Lett.* **34**, L23606 (2007).
30. M. S. Lozier, V. Roussenov, M. S. C. Reed, R. G. Williams, *Nat. Geosci.* **3**, 728 (2010).
31. J. Willis, *Geophys. Res. Lett.* **37**, L06602 (2010).

**Acknowledgments:** This work was supported by the Bundesministerium für Bildung und Forschung North Atlantic project (D.M.) and the Deutsche Forschungsgemeinschaft-funded Cluster of Excellence CliSAP (J.B. and W.A.M.). We thank M. Giorgetta, U. Mikolajewicz, and B. Stevens for comments on the manuscript. All model simulations were performed at the German Climate Computing Centre (DKRZ). Data from the RAPID-WATCH MOC monitoring project are funded by the Natural Environment Research Council and are freely available from [www.noc.soton.ac.uk/rapidmoc](http://www.noc.soton.ac.uk/rapidmoc).

#### Supporting Online Material

[www.sciencemag.org/cgi/content/full/335/6064/76/DC1](http://www.sciencemag.org/cgi/content/full/335/6064/76/DC1)

Materials and Methods

SOM Text

Figs. S1 to S7

References

24 June 2011; accepted 21 November 2011

10.1126/science.1210299

mental and evolutionary origin (7, 8). The ant genus *Pheidole* is one of the most species-rich genera, with 1100 species worldwide (10, 11). All *Pheidole* species have two worker subcastes: minor workers (Fig. 1C) that perform most tasks in the nest and forage and soldiers (Fig. 1B) that

## Ancestral Developmental Potential Facilitates Parallel Evolution in Ants

Rajendran Rajakumar,<sup>1</sup> Diego San Mauro,<sup>1\*</sup> Michiel B. Dijkstra,<sup>1†</sup> Ming H. Huang,<sup>2</sup> Diana E. Wheeler,<sup>2</sup> Francois Hiou-Tim,<sup>1</sup> Abderrahman Khila,<sup>1‡</sup> Michael Cournoyea,<sup>1§</sup> Ehab Abouheif<sup>1||</sup>

Complex worker caste systems have contributed to the evolutionary success of advanced ant societies; however, little is known about the developmental processes underlying their origin and evolution. We combined hormonal manipulation, gene expression, and phylogenetic analyses with field observations to understand how novel worker subcastes evolve. We uncovered an ancestral developmental potential to produce a “supersoldier” subcaste that has been actualized at least two times independently in the hyperdiverse ant genus *Pheidole*. This potential has been retained and can be environmentally induced throughout the genus. Therefore, the retention and induction of this potential have facilitated the parallel evolution of supersoldiers through a process known as genetic accommodation. The recurrent induction of ancestral developmental potential may facilitate the adaptive and parallel evolution of phenotypes.

The wingless worker caste, a universal feature of ants (1, 2), has repeatedly expanded into a complex system of morphologi-

cal and behavioral subcastes. The existence of these subcastes has long fascinated biologists (3–9), yet little is known about their develop-

<sup>1</sup>Department of Biology, McGill University, 1205 Avenue Dr. Penfield, Montreal, Quebec, Canada, H3A 1B1. <sup>2</sup>Department of Entomology, University of Arizona, Forbes 410, Post Office Box 2100: (36), Tucson, AZ 85721–0036, USA.

\*Present address: Biodiversity Research Institute UB (IRBio), Department of Animal Biology, University of Barcelona, Avenida Diagonal 643, E-08028 Barcelona, Spain.

†Present address: Department of Ecology and Evolution, University of Lausanne, Quartier Sorge, “Le Biophore,” CH-1015 Lausanne, Switzerland.

‡Present address: Institut de Genomique Fonctionnelle de Lyon, Ecole Normale Supérieure, CNRS UMR 5242, 46 Allée d’Italie, 69364 Lyon Cedex 07, France.

§Present address: Institute for the History and Philosophy of Science and Technology, University of Toronto, Victoria College 316, 91 Charles Street West, Toronto, Ontario, Canada, M5S 1K7.

||To whom correspondence should be addressed. E-mail: ehab.abouheif@mcgill.ca

defend the nest and process food (11). This complex worker caste system is thought to have promoted the remarkable diversification of *Pheidole* by enhancing the division of labor (11).

In a wild *P. morrissi* colony, we discovered several anomalous soldier-like individuals. These individuals are anomalous because they are significantly larger than normal soldiers (Fig. 2, A and B, and fig. S1), and unlike normal soldiers, they have mesothoracic wing vestiges (Fig. 2, C and D) and rarely occur in nature. These anomalous soldiers are similar to a supersoldier subcaste, which is known to be continually produced in eight *Pheidole* species (fig. S2) (10–12). These species co-occur with army ants and live exclusively in the deserts of the American southwest and northern Mexico (11). In one of these species, *P. obtusospinosa* (Fig. 2, E and I), a major function of the supersoldier subcaste is to block the nest entrance with their extra-large heads and engage in combat to defend against army ant raids (13).

The similarity between the supersoldier-like anomalies in *P. morrissi* and the supersoldier subcaste suggests that they share a developmental origin. Normal soldier development in *Pheidole* may provide insight into how supersoldier-like anomalies may have originated. The soldier subcaste is determined late in larval development at a soldier-minor worker switch point (Fig. 1), which is largely controlled by nutrition (5) and mediated by juvenile hormone (JH) (14, 15). Soldier development is defined by two features: (i) Soldier-determined larvae grow larger than minor worker larvae; and (ii) they develop a pair of vestigial forewing discs in their mesothoracic segment (Fig. 1, E and F) (14–16). These discs show a soldier-specific expression of *spalt* (*sal*) (Fig. 1E) (1), a key gene in the network underlying wing polyphenism in *Pheidole*. *Sal* is a key gene because its expression is spatiotemporally associated with the induction of apoptosis in these vestigial forewing discs (17, 18). Therefore, the supersoldier-like anomalies we found in *P. morrissi* were likely to have originated from the abnormal growth of soldier larvae and their vestigial wing discs. Based on this insight, we predicted that the evolution of the supersoldier subcaste in *Pheidole* occurred through developmental changes that elaborated these two features.

We tested this prediction in *P. obtusospinosa* and *P. rhea*, two species that have a supersoldier subcaste (11). As predicted, their supersoldier larvae grow larger (Fig. 2, F and J, and fig. S3, B and F) and develop two pairs of large vestigial wing discs relative to their soldier larvae (Fig. 2, G and K, and fig. S3, C and G). Furthermore, vestigial wing discs in supersoldier larvae show an elaborated pattern of *sal* expression in the wing pouch relative to those of soldier larvae (Fig. 2, H and L, and fig. S3, D and H, black arrows). We then resolved the evolutionary history of their supersoldier subcaste by reconstructing a phylogeny of 11 *Pheidole* species (fig. S5). Of these, only *P. obtusospinosa* and *P. rhea* have a supersol-

dier subcaste. Our phylogenetic analysis suggests that the supersoldier subcaste has evolved independently, because *P. rhea* is one of the most basal species of this genus, whereas *P. obtusospinosa* is derived (fig. S5) (10). Therefore, the supersoldier subcaste has evolved in parallel, because similar developmental changes underlie its inde-

pendent evolution in *P. obtusospinosa* and *P. rhea*. Furthermore, our phylogenetic analysis suggests that, relative to *P. obtusospinosa*, there are six basal and four derived species (fig. S5). We found that soldier larvae of these basal and derived species differ in their vestigial wing disc number and wing pouch expression of *sal* (fig. S6). This indi-

**Fig. 1.** Wing polyphenism in *P. morrissi*: the ability of a single genome to produce (A) winged queens and wingless (B) soldiers and (C) minor workers (2). Caste determination occurs at two JH-mediated switch points in response to environmental cues (1, 15, 30). (D) Wing discs in queen larvae showing conserved hinge and pouch expression of *sal*. (E) Vestigial wing discs in soldier larvae showing a soldier-specific pattern of *sal* expression, where it is conserved in the hinge but down-regulated in the pouch. Asterisks represent the absence of visible wing discs and *sal* expression in (E) soldier and (F) minor worker larvae. Scale bars indicate the relative sizes of queen, soldier, and minor worker larvae and adults.

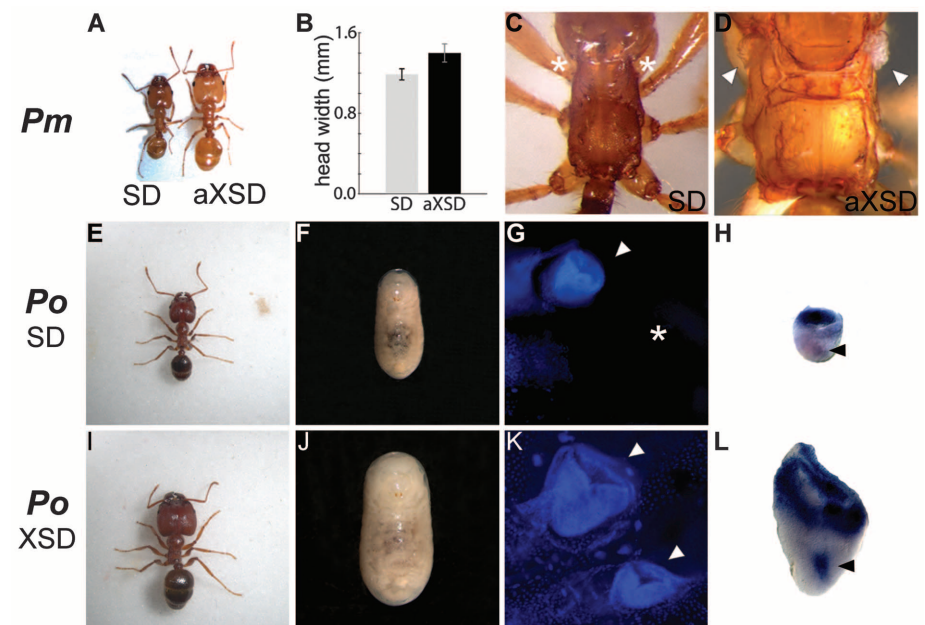
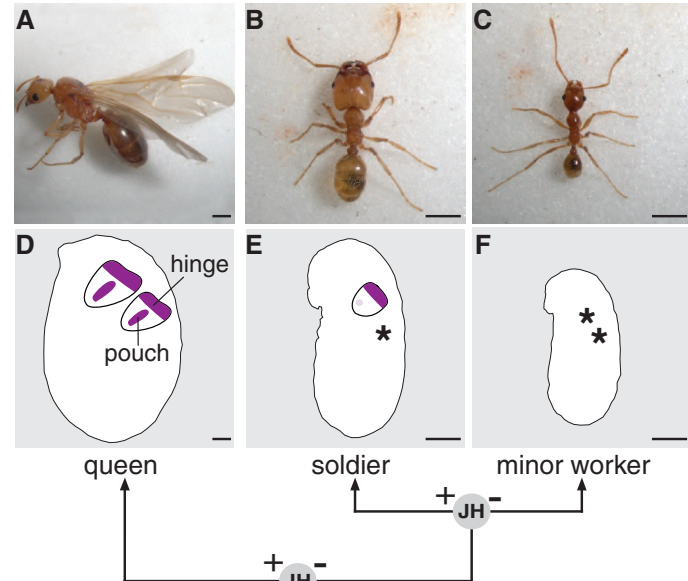


**Fig. 2.** Comparison of *P. morrissi* (Pm) ants: (A, left) Normal adult soldier (SD) and (A, right) anomalous supersoldier (aXSD). (B) Mean and standard deviation of head width of normal SD (gray) and aXSD (black) (fig. S1), and thorax of (C) a normal SD and (D) an aXSD. Comparison of *P. obtusospinosa* (Po) ants: adults of (E) SD and (I) supersoldier (XSD); larvae of (F) SD and (J) XSD; and vestigial wing discs [stained with 4',6-diamidino-2-phenylindole (DAPI)] and *sal* expression in SD (G and H and fig. S4A) and XSD (K and L and fig. S4B). White arrowheads indicate the presence of mesothoracic vestigial wing buds or discs; asterisks denote their absence. Black arrowheads indicate *sal* expression in the wing pouch. Adult, larval, and vestigial wing disc images are all to scale. See fig. S3 for a comparison of *P. rhea* SD and XSD.

cates that the supersoldier subcaste has evolved in parallel despite the evolutionary divergence of soldier development.

Application of methoprene (a JH analog) to *Phenidole* larvae has been shown to induce the development of unusually large soldier pupae (15). In *P. morrisi*, we found that methoprene can induce the development of larvae and adults that mimic the anomalous supersoldier-like individuals of *P. morrisi* and the supersoldiers of *P. obtusospinosa* and *P. rhea*. First, induced

supersoldier larvae (Fig. 3G) and adults (Fig. 3B) are significantly larger than untreated controls (Fig. 3, D and A, and fig. S7), and several of the induced adult supersoldiers have mesothoracic wing vestiges (Fig. 3C). Second, the relative size ranges of induced supersoldiers overlap with those of anomalous and naturally produced supersoldiers (fig. S8). Finally, we found vestigial wing discs of induced supersoldier larvae (Fig. 3, H and I, and fig. S9, B to D and F to H) that mimic those of supersoldier larvae in *P. obtusospinosa* (Fig. 2,

K and L) and *P. rhea* (fig. S3, G and H). Therefore, although *P. morrisi* lacks a supersoldier subcaste, there is a developmental potential to produce supersoldiers that can be induced through JH. Furthermore, the occurrence of supersoldier-like anomalies in *P. morrisi* (Fig. 2A) and other *Phenidole* species (16) suggests that this potential is recurrently induced in nature. This recurrent induction, which is probably mediated by JH, may be caused by nutrition, because it has been shown that environmental variation in nutrition (3) and experimentally increasing nutrition (5) produces supersoldier-like anomalies in *Phenidole* colonies.

We discovered that this developmental potential to produce supersoldiers can be induced by methoprene in other derived (*P. hyatti*) and basal (*P. spadonia*) *Phenidole* species that lack a supersoldier subcaste. As in *P. morrisi*, we found vestigial wing discs of induced supersoldier larvae in *P. hyatti* (fig. S9, J and N) and *P. spadonia* (fig. S9, R and V) that mimic those of supersoldier larvae in *P. obtusospinosa* (Fig. 2, K and L) and *P. rhea* (fig. S3, G and H). Therefore, the developmental potential to produce supersoldiers has been retained and was probably present in the common ancestor of all *Phenidole* (Fig. 4). Without a priori knowledge of this ancestral developmental potential, we would have inferred that the supersoldier subcaste has evolved de novo: once in *P. rhea* and once in *P. obtusospinosa* (fig. S5) (10). However, our results support an alternative explanation for the parallel evolution of supersoldiers: The developmental potential and phenotypic expression of a novel supersoldier subcaste originated in the common ancestor of all *Phenidole* (Fig. 4, section i); the phenotypic expression of supersoldiers was subsequently lost, but the ancestral potential to produce them was retained (Fig. 4, section ii); and this potential was then actualized in *P. obtusospinosa*, leading to the re-evolution of a supersoldier subcaste (Fig. 4, section iii).

Finally, we showed that this ancestral potential was actualized in *P. obtusospinosa* through the re-evolution of a second JH-sensitive period mediating a soldier-supersoldier switch point (fig. S10). We applied methoprene to larvae that had passed the soldier-minor worker switch point but whose caste fate as either soldiers or supersoldiers was still undetermined. We found that applying methoprene to these larvae induced the development of a significantly greater proportion of supersoldiers (fig. S11). Collectively, our results indicate that the supersoldier subcaste in *P. obtusospinosa* re-evolved through genetic accommodation. This process occurs when: (i) a novel phenotype is induced and (ii) this phenotype is incorporated into the population through selection on genes that control its frequency and form of expression (19, 20). Environmental induction of the ancestral potential may have recurrently produced supersoldier-like anomalies in *P. obtusospinosa*. These anomalies would persist, because colonies of *Phenidole* generally care for and buffer anomalies against purifying

**Fig. 3.** Methoprene-induced supersoldiers (iXSD) in *P. morrisi* (*Pm*): comparison of (A) normal SD with (B) iXSD. (C) Thorax of an iXSD. Comparison of (D) SD and (G) iXSD larvae, and of vestigial wing discs (stained with DAPI) and *sal* expression in (E and F) normal SD and (H and I) iXSD. White arrowheads indicate the presence of mesothoracic vestigial wing buds or discs; asterisks denote their absence. Black arrowheads indicate *sal* expression in the wing pouch. Adult, larval, and vestigial wing disc images are all to scale.

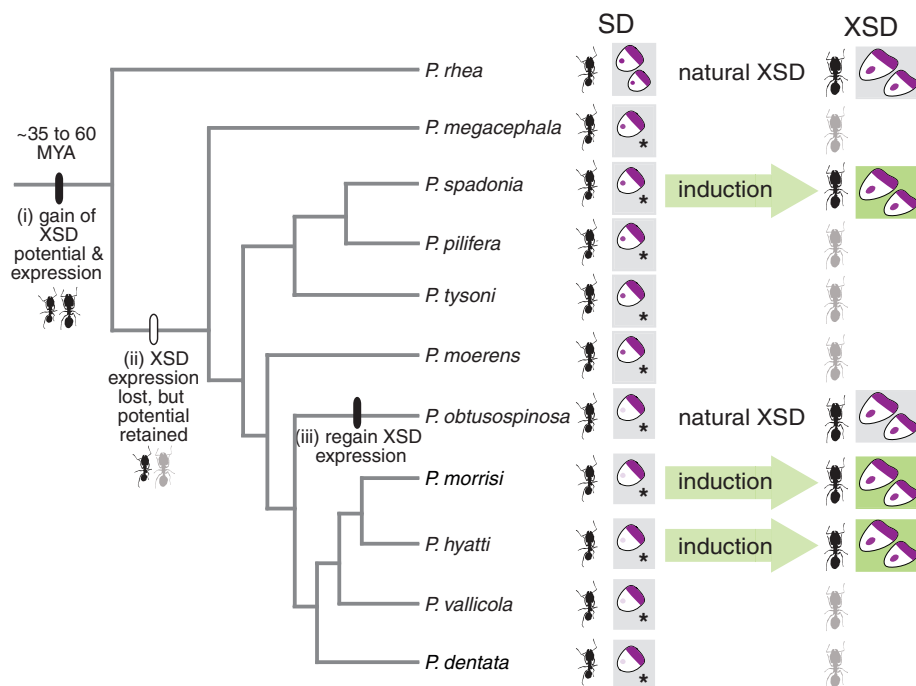
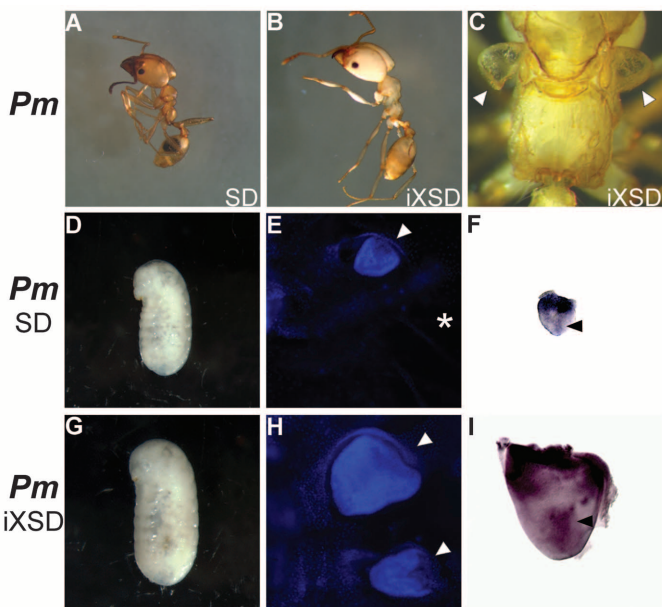


**Fig. 4.** Evolutionary history of ancestral developmental potential and phenotypic expression of supersoldiers (XSDs). MYA, million years ago. Purple represents the pattern of *sal* expression; asterisks indicate the absence of vestigial wing discs and *sal* expression. Green arrows and boxes represent the induction of XSD potential.

selection (3). Selection on *P. obtusospinosa* colonies may have incorporated induced supersoldier-like anomalies by increasing their frequency through modification of the JH system (fig. S12) and by inhibiting the formation of any wing vestiges (fig. S13 and S14). Army ant raids may have been a selective pressure that incorporated these anomalies, because *P. obtusospinosa* supersoldiers currently use their extra-large heads to defend against these raids (13).

Selection for re-evolving supersoldiers may generally be reduced, because almost all *Pheidole* species lack a supersoldier subcaste (10, 11). *P. hyatti* provides insight into how this selective pressure can be reduced: Although *P. hyatti* retains the developmental potential (Fig. 4) and lives in an ecological environment similar to that of *P. obtusospinosa*, it has not re-evolved a supersoldier subcaste (11). Instead, *P. hyatti* uses nest evacuation behavior when attacked by army ants (21). The retention of this potential in *P. hyatti* and other *Pheidole* species that lack a supersoldier subcaste may therefore be due to a clade-specific constraint (22). This constraint may have arisen from having the same hormone (JH) mediate the determination of both soldiers and supersoldiers in the common ancestor of all *Pheidole*. Soldiers and supersoldiers are both defined by their larval size and the development of their vestigial wing discs, which indicates that their developmental programs share many modules. Therefore, the ancestral potential to produce supersoldiers cannot be lost without compromising the developmental program of soldiers.

Recurrent phenotypes reflecting ancestral potentials have long been recognized as widespread in plants and animals (6, 19, 23–28). Because of the lack of empirical evidence, however, the evolutionary significance of these recurrent phenotypes has been underappreciated (19, 29). We uncovered an ancestral developmental potential to produce a novel supersoldier subcaste that has been retained throughout a hyperdiverse ant genus that evolved ~35 to 60 million years ago (10) (Fig. 4). Our results suggest that the recurrent induction of ancestral developmental potential is an important source of adaptive variation for selection that facilitates the adaptive and parallel evolution of novel phenotypes.

#### References and Notes

1. E. Abouheif, G. A. Wray, *Science* **297**, 249 (2002).
2. B. Hölldobler, E. O. Wilson, *The Ants* (The Belknap Press of Harvard Univ. Press, Cambridge, MA, 1990).
3. W. M. Wheeler, *Science* **15**, 766 (1902).
4. R. Gregg, *Ecology* **23**, 295 (1942).
5. W. Goetsch, *Naturwissenschaften* **25**, 803 (1937).
6. C. Darwin, *On the Origin of Species* (J. Murray, London, 1859).
7. E. O. Wilson, *Q. Rev. Biol.* **28**, 136 (1953).
8. D. E. Wheeler, *Am. Nat.* **128**, 13 (1986).
9. B. Hölldobler, E. O. Wilson, *The Superorganism* (W. W. Norton, New York, 2009).
10. C. S. Moreau, *Mol. Phylogenet. Evol.* **48**, 224 (2008).
11. E. O. Wilson, *Pheidole in the New World* (Harvard Univ. Press, Cambridge, MA, 2003).
12. M. H. Huang, D. E. Wheeler, *Insects Soc.* **58**, 539 (2011).
13. M. H. Huang, *J. Insect Sci.* **10**, 1 (2010).
14. D. E. Wheeler, H. F. Nijhout, *Science* **213**, 361 (1981).
15. D. E. Wheeler, H. F. Nijhout, *J. Insect Physiol.* **29**, 847 (1983).
16. D. E. Wheeler, H. F. Nijhout, *Int. J. Insect Morphol. Embryol.* **10**, 131 (1981).
17. S. J. Shbalat, A. Khila, E. Abouheif, *Evol. Dev.* **12**, 580 (2010).
18. S. Y. Sameshima, T. Miura, T. Matsumoto, *Evol. Dev.* **6**, 336 (2004).
19. M. J. W. Eberhard, *Developmental Plasticity and Evolution* (Oxford Univ. Press, New York, 2003).
20. Y. Suzuki, H. F. Nijhout, *Science* **311**, 650 (2006).
21. R. Droual, *Behav. Ecol. Sociobiol.* **12**, 203 (1983).
22. S. C. Stearns, *Acta Palaeontol. Pol.* **38**, 215 (1994).
23. A. E. Bely, J. M. Sikes, *Proc. Natl. Acad. Sci. USA* **107**, 1464 (2010).
24. C. C. Ledon-Rettig, D. W. Pfennig, N. Nascone-Yoder, *Evol. Dev.* **10**, 316 (2008).
25. A. Meyer, in *Homology*, G. R. Bock, G. Cardew, Eds. (Wiley, London, 1999), vol. 22, pp. 141–157.
26. M. P. Harris, S. M. Hasso, M. W. J. Ferguson, J. F. Fallon, *Curr. Biol.* **16**, 371 (2006).
27. W. S. Armbruster, J. Lee, B. G. Baldwin, *Proc. Natl. Acad. Sci. USA* **106**, 18085 (2009).
28. W. Goetsch, *Zool. Anz.* **128**, 209 (1939).
29. M. L. J. Stiassny, in *Keywords and Concepts in Evolutionary Developmental Biology* (Harvard Univ. Press, Cambridge, MA, 2003), pp. 10–14.
30. L. Passera, J. P. Suzzoni, *Insects Soc.* **26**, 343 (1979).

**Acknowledgments:** We thank R. Sanwald, R. Johnson, S. Cover, M. Seid, W. Tschanke, and J. King for help with ant collection or identification; Wellmark for methoprene; and T. Flatt, G. Wray, C. Metz, S. Jolie, Abouheif lab members, and Konrad Lorenz Institute (KLI) fellows for comments. This work was supported by a Natural Sciences and Engineering Research Council grant and a KLI fellowship to E.A., as well as grants from NSF (0344946) and the Arizona Agricultural Experiment Station (ARZT 136321-H3106) to D.E.W. DNA sequences were deposited in GenBank (accession nos. JN205075 to JN205109).

#### Supporting Online Material

[www.sciencemag.org/cgi/content/full/335/6064/79/DC1](http://www.sciencemag.org/cgi/content/full/335/6064/79/DC1)

Materials and Methods

Figs. S1 to S16

Tables S1 to S2

References (31–46)

20 July 2011; accepted 22 November 2011

10.1126/science.1211451

*Caenorhabditis elegans*. We used a transgene to overexpress the transcription factor heat shock factor 1 (HSF-1), a master regulator of the environmental stress response. Transgenic animals are more resistant to a range of environmental challenges (18, 19) and show a delayed age-dependent reduction in protein-folding homeostasis (20). We crossed the *hsf-1* transgenic animals with strains carrying diverse mutations that affect development but with outcomes that vary across individuals (table S1).

In 8 out of 11 tested cases, mutation penetrance was reduced in the transgenic animals (Fig. 1, fig. S1, and table S2). Protection was observed for mutations affecting both embryonic (Fig. 1A) and postembryonic (Fig. 1B) development. For example, embryonic lethality caused by a deletion in the intermediate filament protein gene *ifb-1* reduced from 33% to 17% (48% of animals that would have died were protected,  $P = 5.7 \times 10^{-12}$ ) (Fig. 1, fig. S1, and table S4). The buffered mutations are molecularly diverse and act in distinct

<sup>1</sup>European Molecular Biology Laboratory—Center for Genomic Regulation (EMBL-CRG) Systems Biology Unit, CRG and Universitat Pompeu Fabra, Barcelona, Spain. <sup>2</sup>Institució Catalana de Recerca i Estudis Avançats (ICREA), CRG and Universitat Pompeu Fabra, Barcelona, Spain.

\*To whom correspondence should be addressed. E-mail: ben.lehner@crg.eu

## Fitness Trade-Offs and Environmentally Induced Mutation Buffering in Isogenic *C. elegans*

M. Olivia Casanueva,<sup>1</sup> Alejandro Burga,<sup>1</sup> Ben Lehner<sup>1,2\*</sup>

Mutations often have consequences that vary across individuals. Here, we show that the stimulation of a stress response can reduce mutation penetrance in *Caenorhabditis elegans*. Moreover, this induced mutation buffering varies across isogenic individuals because of interindividual differences in stress signaling. This variation has important consequences in wild-type animals, producing some individuals with higher stress resistance but lower reproductive fitness and other individuals with lower stress resistance and higher reproductive fitness. This may be beneficial in an unpredictable environment, acting as a “bet-hedging” strategy to diversify risk. These results illustrate how transient environmental stimuli can induce protection against mutations, how environmental responses can underlie variable mutation buffering, and how a fitness trade-off may make variation in stress signaling advantageous.

**A** specific mutation can have different consequences in different individuals. For example, even in “Mendelian” human diseases, such as cystic fibrosis, an inherited mutation can result in severe disease in one individual but a milder phenotype in another (1). Incomplete penetrance is also observed in isogenic model organisms and is poorly understood (2–4).

Many mutations have outcomes that depend on the activity of molecular chaperones—

proteins that aid the folding of other macromolecules (5–14). More generally, molecular mechanisms that promote environmental robustness (survival after environmental challenges) also tend to increase mutational robustness [the extent to which an organism’s phenotype remains constant in spite of mutation (15–17)].

We investigated whether genetically increasing environmental stress resistance could modify mutation penetrance in the model organism



## Ancestral Developmental Potential Facilitates Parallel Evolution in Ants

Rajendran Rajakumar, Diego San Mauro, Michiel B. Dijkstra, Ming H. Huang, Diana E. Wheeler, Francois Hiou-Tim, Abderrahman Khila, Michael Cournoyea and Ehab Abouheif  
(January 5, 2012)

*Science* **335** (6064), 79-82. [doi: 10.1126/science.1211451]

Editor's Summary

### Supersoldier Throwbacks

Anomalous traits reflecting those of an ancestor sporadically appear in individuals that normally should not have them. Through their work with the hyperdiverse ant genus *Pheidole*, **Rajakumar et al.** (p. 79) suggest that these anomalies represent raw materials for selection to act upon. The ants possess an ancestral developmental potential, to produce "supersoldiers," that has been retained for over 30 million years for which recurrent induction has facilitated the adaptive and parallel evolution of supersoldiers.

---

This copy is for your personal, non-commercial use only.

---

#### Article Tools

Visit the online version of this article to access the personalization and article tools:  
<http://science.sciencemag.org/content/335/6064/79>

#### Permissions

Obtain information about reproducing this article:  
<http://www.sciencemag.org/about/permissions.dtl>



[www.sciencemag.org/cgi/content/full/335/6064/79/DC1](http://www.sciencemag.org/cgi/content/full/335/6064/79/DC1)

## Supporting Online Material for

### **Ancestral Developmental Potential Facilitates Parallel Evolution in Ants**

Rajendran Rajakumar, Diego San Mauro, Michiel B. Dijkstra, Ming H. Huang, Diana E. Wheeler, Francois Hiou-Tim, Abderrahman Khila, Michael Cournoyea, Ehab Abouheif\*

\*To whom correspondence should be addressed. E-mail: ehab.abouheif@mcgill.ca

Published 6 January 2012, *Science* **335**, 79 (2012)

DOI: 10.1126/science.1211451

#### This PDF file includes:

- Materials and Methods
- Figs. S1 to S16
- Tables S1 and S2
- References (31–47)

## SUPPORTING ONLINE MATERIAL

### Materials and Methods

**Animal collection and culturing.** We collected queen-right colonies of *P. morrissi*, *P. tysoni*, *P. pilifera* from Long Island, New York, USA, and *P. rhea*, *P. obtusospinosa*, *P. hyatti*, *P. spadonia*, and *P. vallicola* from the southwest of Arizona, USA, and *P. dentata*, *P. megacephala*, and *P. moerens*, from Tallahassee, Gainesville, and Fort Lauderdale, Florida, USA. Colonies were maintained in plastic boxes with glass test tubes filled with water constrained by cotton wool, and were fed a combination of mealworms, cockroaches, crickets, sunflower seed, and Bhatkar-Whitcomb diet (31). All colonies were maintained at 27 °C, 70% humidity, and 12 hour day:night cycle.

**Isolation of *sal* homologues.** We isolated fragments of *sal* from *P. morrissi* (1), as well as from *P. obtusospinosa* and *P. rhea* using PCR on cDNA that was generated from reverse transcription of their larval mRNA. We cloned and sequenced these fragments to confirm their identity, and performed gene tree analyses to confirm their orthology with *Nasonia*, *Apis*, and *Drosophila sal*. PCR primers and conditions are described in (1). GenBank accession numbers are JN205075 for *P. obtusospinosa sal* and JN205076 for *P. rhea sal*.

**Whole mount *in situ* hybridization and immunohistochemistry.** We fixed and processed last instar larvae just prior to the prepupal stage (32). We carefully dissected larvae under a Zeiss Discovery V12 stereomicroscope to remove obstructive tissues surrounding imaginal discs. We then synthesized a digoxigenin-labelled riboprobe (Roche Diagnostics Canada) for *P. morrissi sal* (33). We used this *P. morrissi sal* probe for all *in situ*

hybridizations because: (i) *sal* sequences in *P. morrisi*, *P. obtusospinosa*, and *P. rhea* are 96% similar to each other (fig. S15); and (ii) the *P. morrisi* *sal* probe cross-reacts and reveals a conserved pattern of *sal* expression in the wing discs of winged castes of the *Pheidole* species used in this study (fig. S16).

**Phylogenetic analyses.** To infer the relationships of the 11 *Pheidole* species included in our study, we performed a Bayesian analysis using MrBayes v3.1.2 (34). Following Moreau (10), *Myrmica incompleta* was used as an outgroup. We isolated, cloned, and sequenced the following fragments using PCR (Table S1): (i) a ~616bp fragment of mitochondrial (mt) protein-coding *cox1*; (ii) a ~744bp fragment of mt protein-coding *cytb*; (iii) a ~535bp fragment of nuclear protein-coding *lwr*. GenBank accession numbers for these sequences are listed in Table S2. Additionally, we retrieved sequences from GenBank for: (i) a ~340bp fragment of nuclear protein-coding *H3*; (ii) a ~360bp fragment of mt ribosomal 12S; and (iii) all sequences for *Myrmica incompleta*. In total, we used approximately 2.6kb of concatenated sequence spanning 5 genes. We initially aligned these sequences using ClustalX v1.83.1 (35), and subsequently adjusted these alignments by eye using McClade v4.06 (36). To determine the optimal model of sequence evolution for each gene, we used AIC criteria within ModelTest v3.7 (37, 38). As a result, we used GTR+Γ+I for *cox1* and *cytb*, GTR+I for *H3*, and GTR+Γ for *lwr* and 12S. Bayesian analysis involved two independent runs and used four Markov chains with an MCMC (Monte Carlo Markov Chain) length of 10,000,000 generations. The chains were sampled every 200 generations following a burn-in period of 1,000,000 generations. Data used for the analysis was partitioned by gene, each of which was assigned a separate substitution

model. The analysis resulted in a sample of trees with a mean likelihood score of  $-\ln L = 12156.91$  for run 1 and  $-\ln L = 12156.95$  for run 2. The average standard split frequencies of the chains after 10,000,000 generations was 0.002391, suggesting that the chains had reached convergence. The trees from both analyses were thus combined and summarized with a fully resolved majority-rule consensus tree.

**Hormonal applications.** We topically applied methoprene (Wellmark International), a juvenile hormone (JH) analogue, to the dorsal abdomens of *Pheidole* larvae. We applied methoprene to *P. morrissi* larvae (range of longest larval lengths was 0.9-1.8mm), *P. spadonia* larvae (1.5-2.7mm), and *P. hyatti* larvae (1.0-1.5mm) prior to their determination as either minor workers or soldiers. For *P. obtusospinosa*, a species that naturally produces supersoldiers, the final size range (longest larval length) is 1.7-2.18mm for minor worker larvae, 3.3-3.6mm for soldier larvae, and 4.1-4.6mm for supersoldier larvae. We therefore applied methoprene to *P. obtusospinosa* larvae that had already passed the soldier-minor worker switch point (2.2-3.3mm), but whose caste fate as either soldiers or supersoldiers had not yet been determined. We applied methoprene at a concentration of 5 mg/ml in acetone to *P. morrissi* larvae, 3 mg/ml in acetone to *P. hyatti* larvae, and both 3.5 mg/ml and 5 mg/ml in acetone to *P. spadonia* and *P. obtusospinosa* larvae. For *P. morrissi*, we followed Wheeler (16) and set-up multiple replicates of 40 methoprene-treated larvae raised by 40 workers and no soldiers. We fixed half of the surviving larvae just prior to the prepupal stage, and we let the other half of surviving larvae continue to develop. As controls, we set up multiple replicates in *P. morrissi* of 40 acetone-treated or untreated larvae raised by 40 workers and no soldiers. To

confirm that methoprene can induce supersoldier larvae in other species that lack supersoldiers, we treated a large number of *P. spadonia* and *P. hyatti* larvae with methoprene and raised them in replicate boxes each of which contained 50-100 minor workers. To test whether a second JH-sensitive period mediates the switch between soldiers and supersoldiers larvae in *P. obtusospinosa*, we treated 200 larvae with methoprene and 200 larvae with acetone only. We raised these methoprene and acetone-treated larvae in replicate boxes, each of which contained 50-100 minor workers. For all experiments, we identified “supersoldier” larvae by finding the smallest larva (shortest larval length in mm) in the sample with two pairs of vestigial wing discs (a defining feature of supersoldier larvae). We then considered any larva longer than this as “supersoldier” larvae. Furthermore, adult *Pheidole* supersoldiers are defined as showing discrete differences from their soldiers in: (i) their head size and/or; (ii) the allometric scaling relation between the size of their heads and size of their bodies (12, 13). Naturally produced supersoldiers in *P. obtusospinosa* have significantly larger heads than their soldiers, whereas in *P. rhea* they have both significantly larger heads and their heads are smaller relative to their bodies than in soldiers (12, 13). We therefore considered adults that were produced by methoprene treatment to be “induced supersoldiers” if their heads were significantly larger than the heads of untreated controls.

### **Statistical analyses and measurement**

We used a Zeiss Discovery V12 stereomicroscope and Zeiss Axiovision software to measure the larval size (body length in mm) and adult size (head width in mm). We used an unequal variances t-test (39, 40) to determine whether in *P. morrisi* the mean size of:

(i) adult minor workers from anomalous colony is equal to that of normal minor workers; (ii) adult anomalous supersoldiers is equal to that of normal soldiers; (iii) methoprene-treated larvae is equal to that of untreated controls; and (iv) adults resulting from methoprene-treated larvae is equal to that of untreated controls. We used a Fisher's exact test (40) to determine whether in *P. obtusospinosa* the proportions of supersoldier relative to soldier larvae in methoprene treatments are equal to the proportions of acetone-treated controls. Finally, we calculated the coefficient of variation to compare the relative amounts of variation (40) in the surface area of fore- and hindwing vestigial discs in normal and methoprene-induced supersoldier larvae in *P. obtusospinosa*, as well as induced supersoldier larvae in *P. morrisi*, *P. hyatti*, and *P. spadonia*.

## Supplementary Figures and Figure Legends

**Fig. S1. Anomalous *P. morrisi* supersoldiers are significantly larger than normal soldiers.** X-axis showing the mean (bars) and standard deviation (error bars) for head widths (mm) of normal minor workers (gray bar, n= 20), minor workers from the anomalous colony (black bar, n = 5), normal soldiers (SD; gray bar, n = 20), and anomolous supersoldier-like individuals (aXSD; black bar, n = 8). An unequal variance t-test (two-tailed) between minor workers from the normal and from the anomalous colony shows that they are not significantly different from one another ( $t = 2.083$ ,  $df = 12$ ,  $P = 0.06$ ). In contrast, an unequal variance t-test (two-tailed) between normal SD and aXSD shows that they are significantly different from one another ( $t = 6.265$ ,  $df = 9$ ,  $P = 0.0002$ ). This shows that aXSD are significantly larger in size than normal soldiers.

**Fig. S1.**

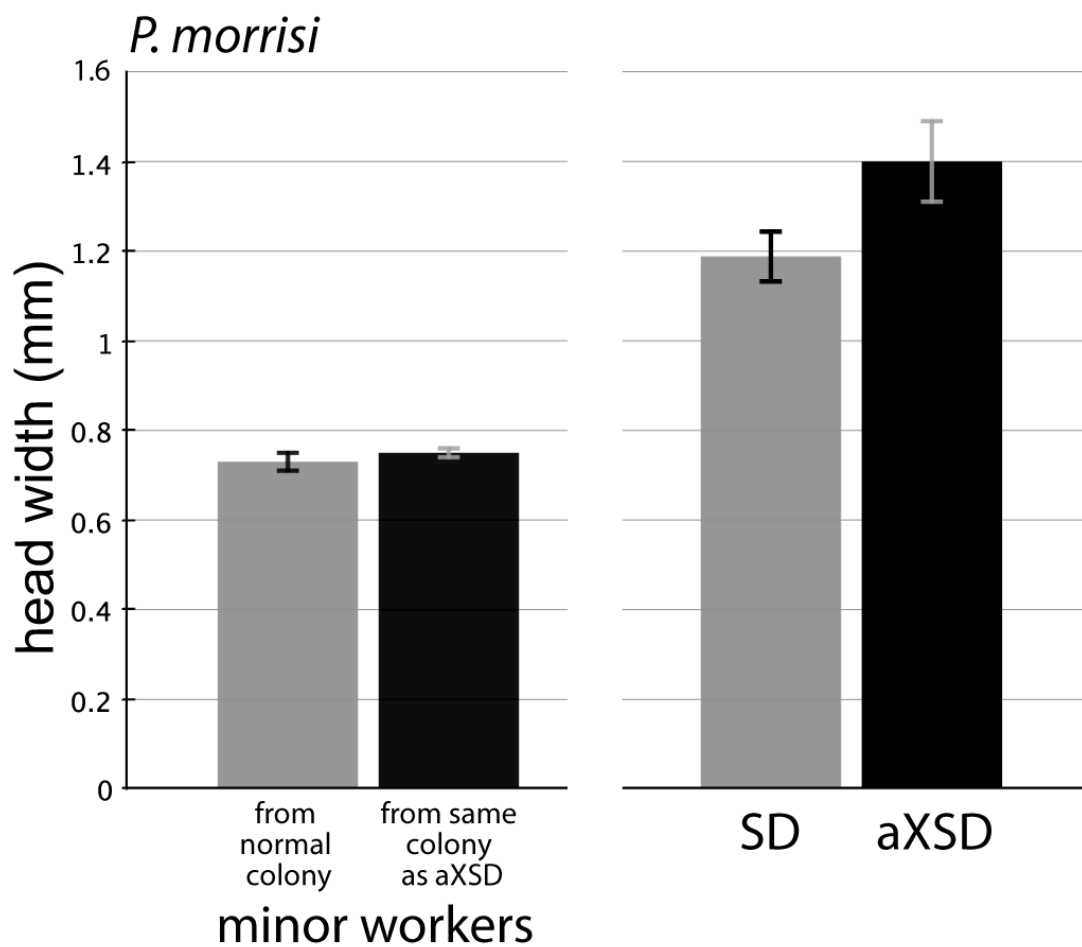
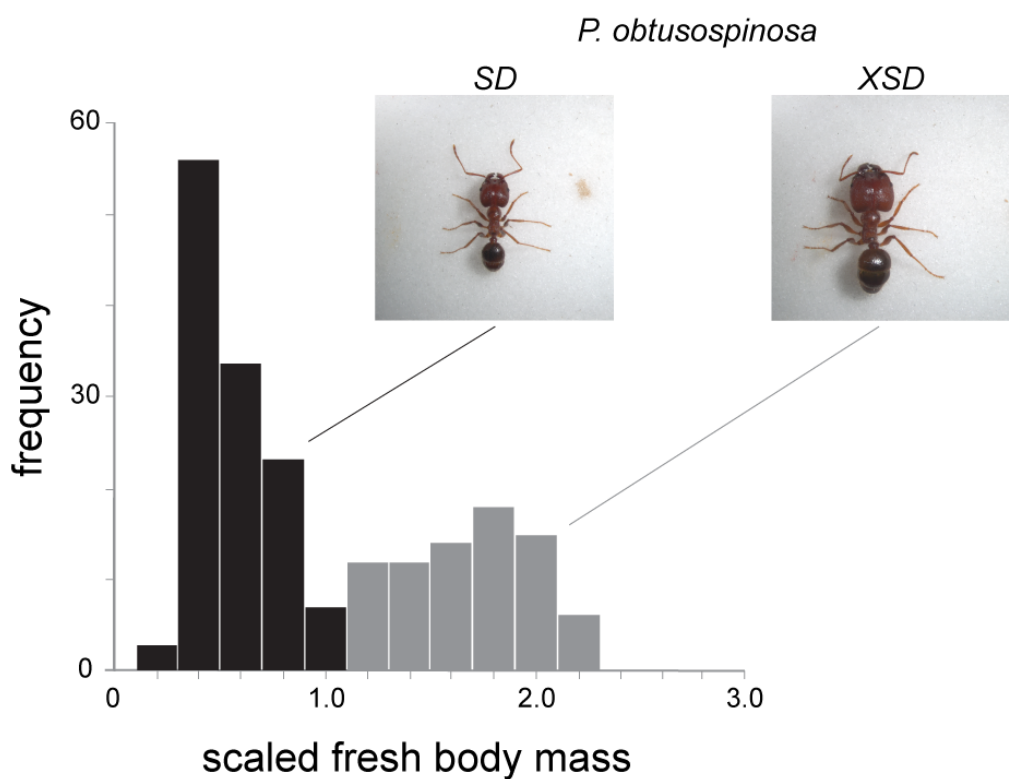


**Fig. S2. Definition and frequency distributions of the supersoldier subcaste in *P.***

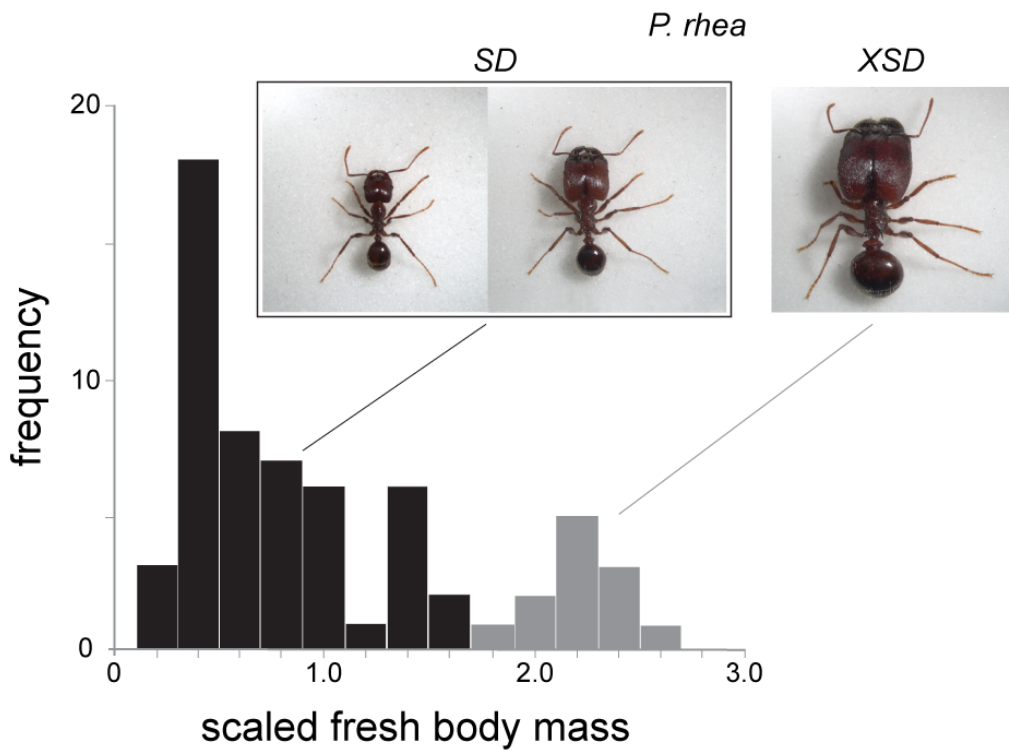
***obtusospinosa* and *P. rhea*.** *Pheidole* supersoldiers (XSD) are defined as showing discrete differences from their soldiers (SD) in: (i) their head size and/or; (ii) the allometric scaling relation between their head and body size (12, 13). In *P. obtusospinosa*, naturally produced XSD have significantly larger heads than their SD (compare SD to XSD in **A**), whereas in *P. rhea* XSD have both significantly larger heads and their heads are smaller relative to their bodies than in SD (compare SD to XSD in **B**) (12, 13). Histograms showing the frequency distributions of soldiers (black bars) and supersoldiers (dark gray bars) based on total fresh body mass for (**A**) *P. obtusospinosa* and (**B**) *P. rhea*. Y-axis: indicates frequency of the soldier and supersoldier subcaste. X-axis: scaled fresh body mass. To facilitate comparing the distributions of *P. obtusospinosa* and *P. rhea*, we scaled fresh body masses of each species by dividing every fresh body mass (mg) by a mean fresh body mass (mg) that was calculated over all supersoldiers and soldiers. All images are to the same scale. These distributions are consistent with those of (12, 13) in showing that the distribution of soldiers in *P. rhea* is much broader than that of *P. obtusospinosa*.

**Fig. S2.**

**A**

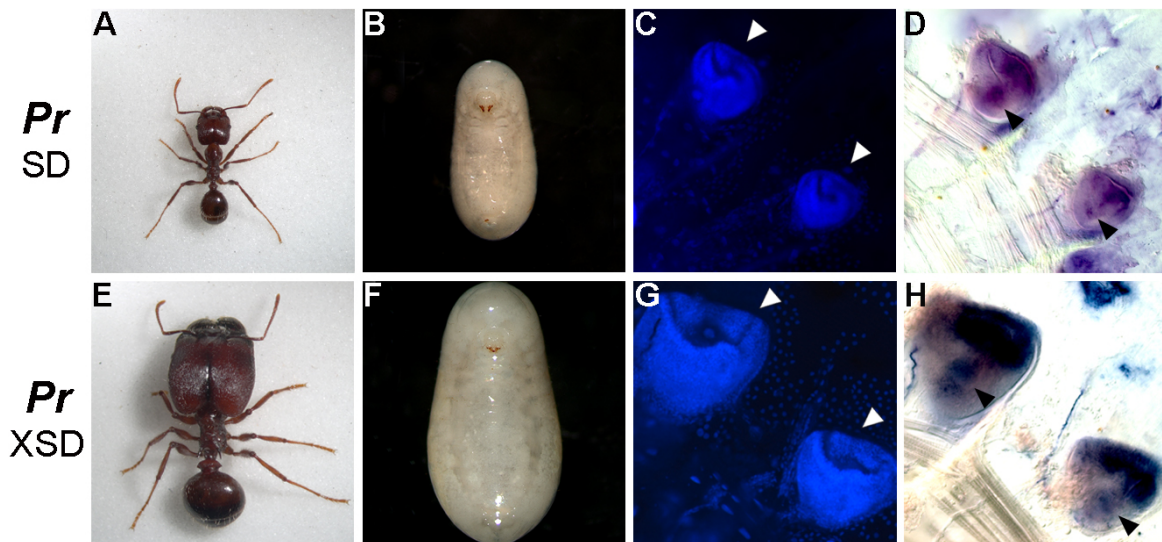


**B**



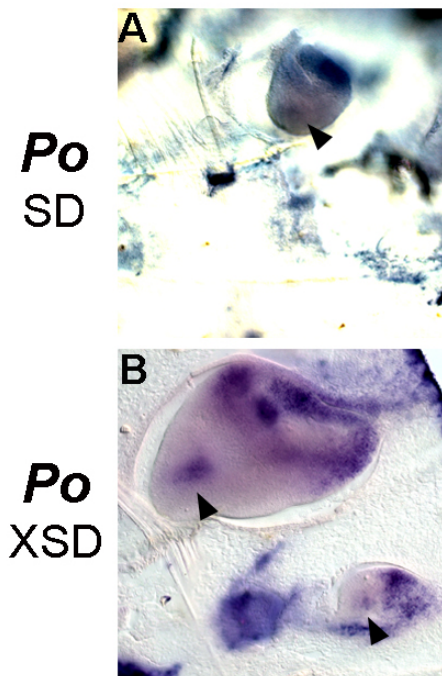
**Fig. S3. Development of supersoldiers in *P. rhea*.** Comparison of adults of (A) SD and (E) XSD as well as larvae of (B) SD and (F) XSD. Comparison of vestigial wing discs (DAPI) and *sal* mRNA expression (purple) of (C and D) SD and (G and H) XSD. White arrowheads indicate presence of mesothoracic wing vestiges or vestigial wing discs, whereas asterisks indicate their absence. Black arrowheads indicate *sal* expression in wing pouch. Adult, larval and vestigial wing disc images are all to scale.

**Fig. S3.**

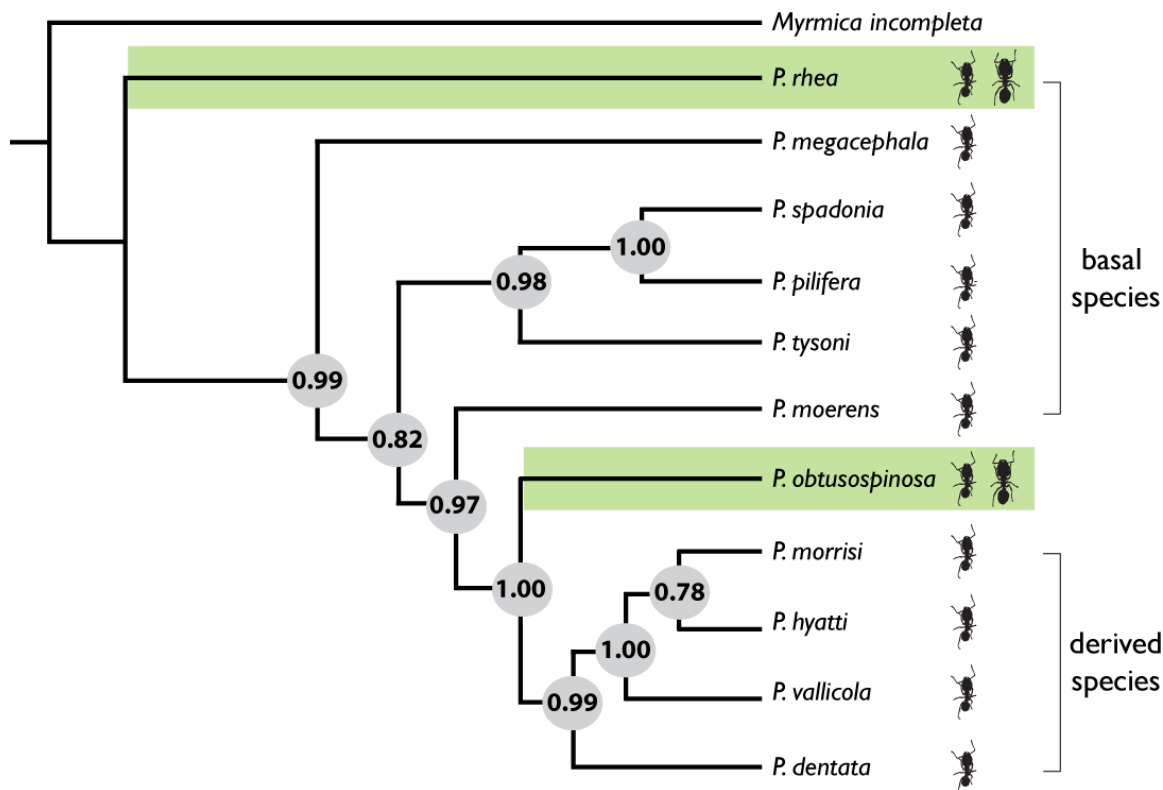


**Fig. S4. Expression of *sal* in vestigial wing discs of soldier and supersoldier larvae in *P. obtusospinosa*.** *sal* mRNA expression (purple) in the vestigial wing discs of *Pheidole obtusospinosa* (*Po*): (A) soldiers (SD) and (B) supersoldiers (XSD). Black arrowheads indicate wing pouch expression of *sal*. Note that, as in *P. morrisi*, *Po* SDs have (A) a single pair of vestigial forewing discs in which *sal* expression is conserved in the hinge region, but is highly downregulated in the wing pouch. (B) *Po* XSDs have both fore- and hindwing discs, in which *sal* expression is conserved in the hinge and elaborated in the wing pouch relative to the expression of *sal* in SD. Both images are to scale.

**Fig. S4.**

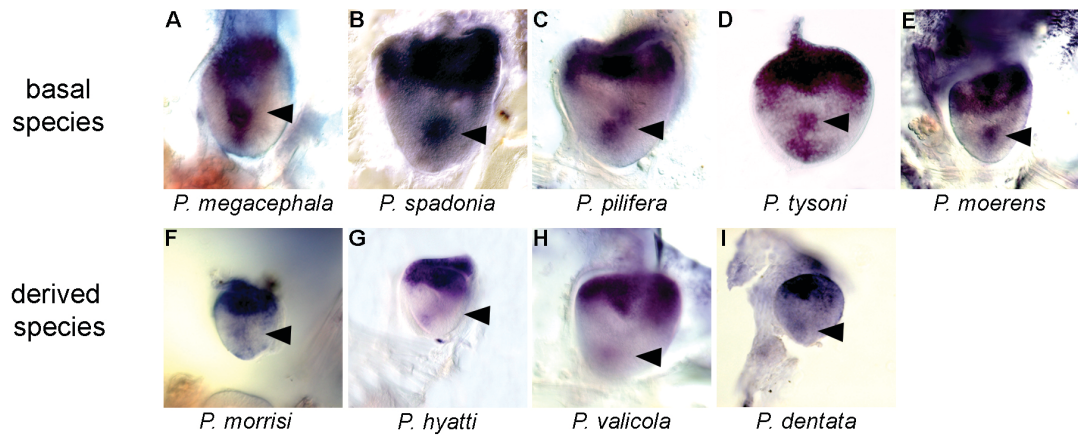


**Fig. S5. Bayesian phylogenetic analysis of the 11 *Pheidole* species we used in this study confirms the independent evolution of supersoldiers of *P. rhea* and *P. obtusospinosa* and provides strong support for their inferred relationships.** Although Moreau (10) reconstructed a genus-level phylogeny using 142 *Pheidole* species, the phylogenetic relationships of the 11 species that we used in this study remained largely unresolved. This greatly decreases our ability to reconstruct the evolutionary history of supersoldiers. We therefore performed a detailed Bayesian phylogenetic analysis of all 11 species to further resolve their relationships and confirm the independent evolution of supersoldiers in *P. rhea* and *P. obtusospinosa*. Our analysis yielded high posterior probabilities for almost all nodes (gray circles) in the tree, which provides substantial confidence in the inferred phylogenetic relationships. Our results are consistent with (10) in that *P. rhea* is supported as a sister taxon of almost all *Pheidole* species as well as one of the most basal species in the genus. Our phylogenetic analysis supports *P. obtusospinosa* as a derived species confirming the independent evolution of supersoldier subcastes (green lines) (10). Our analysis also shows that there are six species that are “basal” and four species that are “derived” relative to *P. obtusospinosa*.

**Fig. S5.**

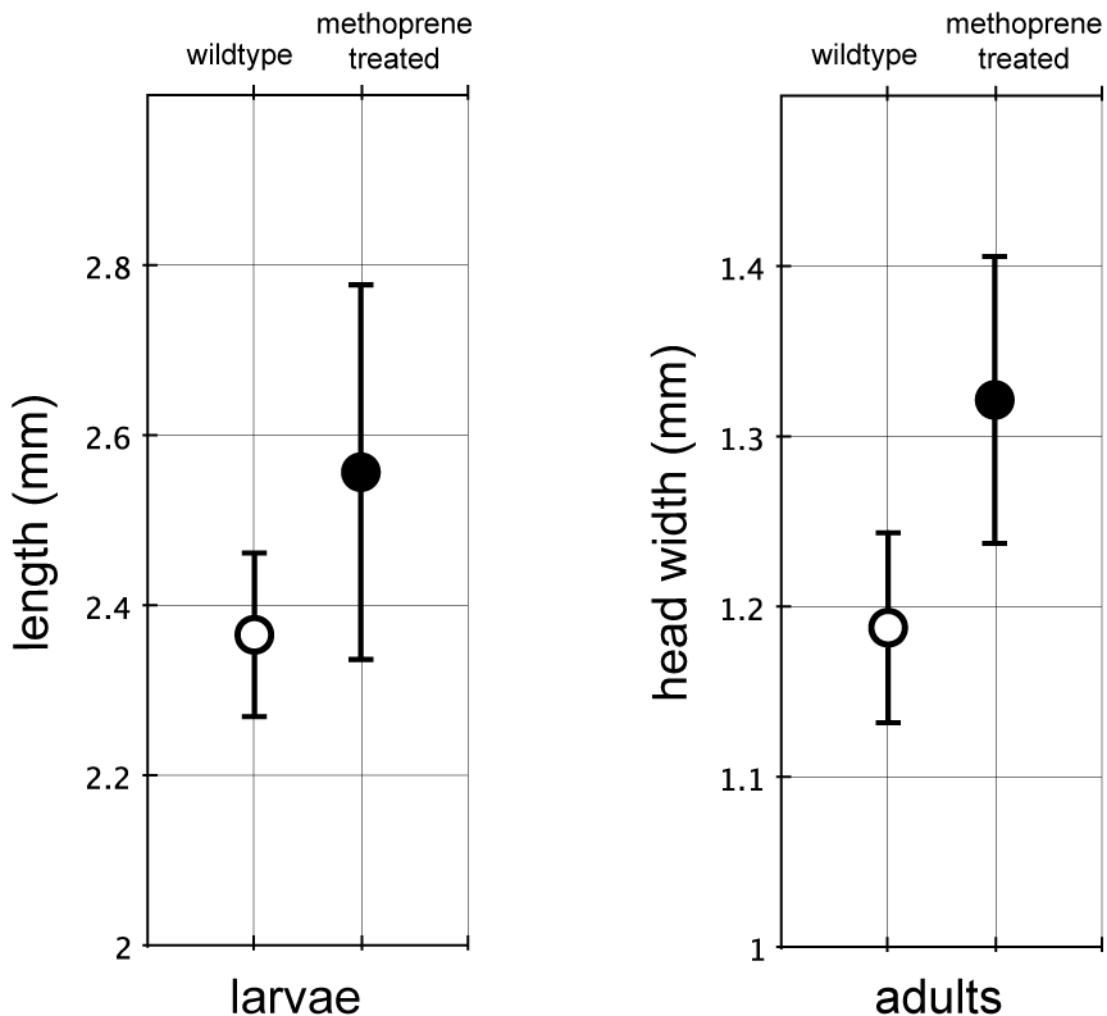
**Fig. S6. Interruption of *sal* expression in soldier forewing discs differs between basal and derived *Pheidole* species.** (A to I), all images are to scale and represent vestigial forewing discs from late final instar soldier larvae. (A to E), *sal* mRNA expression (purple) in vestigial soldier forewing discs of basal *Pheidole* species (fig S5): relative to its expression in the hinge, black arrows indicate *sal* is expressed as a well-defined patch of expression in the wing pouch (see fig S3D for *P. rhea*). (F to I) *sal* expression in vestigial soldier forewing discs of derived *Pheidole* species (fig S5): relative to its expression in the hinge, black arrows indicate *sal* is expressed as a barely visible and diffuse patch of expression in the wing pouch (see figS4A for *P. obtusospinosa*). These differences in *sal* expression, which occur regardless of the size of vestigial forewing discs, reflect genetically fixed differences that have evolved between these basal and derived *Pheidole* species.

**Fig. S6.**

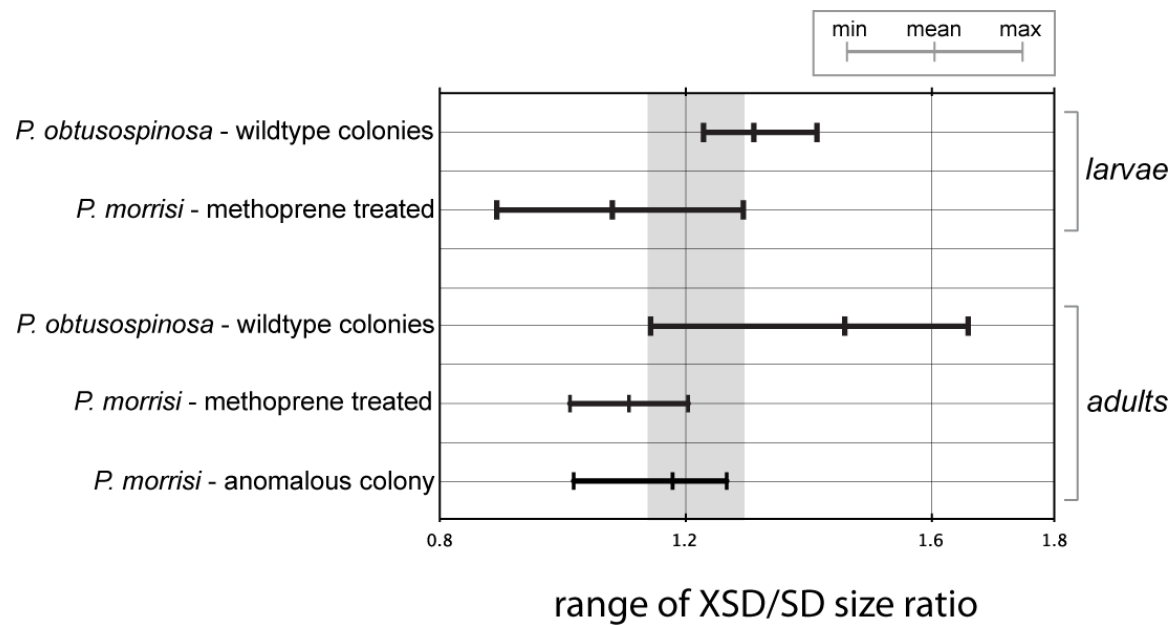


**Fig. S7. Application of methoprene induces the development of supersoldier larvae and adults in *P. morrisi*.** Graph on left shows mean (circles) and standard deviation (error bars) for larval length (mm) of untreated (white circle; n = 50) and methoprene-treated (black circle; n = 36) larvae. The mean for methoprene-treated larvae represents larvae from all replicates. An unequal variances t-test (one-tailed) shows that the mean of methoprene-treated larvae is significantly larger than that of untreated larvae ( $t = 4.887$ ,  $df = 44$ ,  $P < 0.0001$ ). All larvae that survived the acetone-treated controls (n = 24; from all replicates) developed into minor worker larvae. Graph on right shows mean and standard deviation for adult head width (mm) of adults that developed from untreated larvae (white circle; n = 30) and adults that developed from methoprene-treated larvae (black circle; n = 7). The mean for adults that developed from methoprene-treated larvae represents adults from all replicates. An unequal variance t-test (one-tailed) shows that the mean of adults that developed from methoprene-treated larvae is significantly larger than those that were untreated ( $t = 3.742$ ,  $df = 7$ ,  $P = 0.0036$ ). All adults that survived the acetone-treated controls (n = 42 from all replicates) developed into adult minor workers.

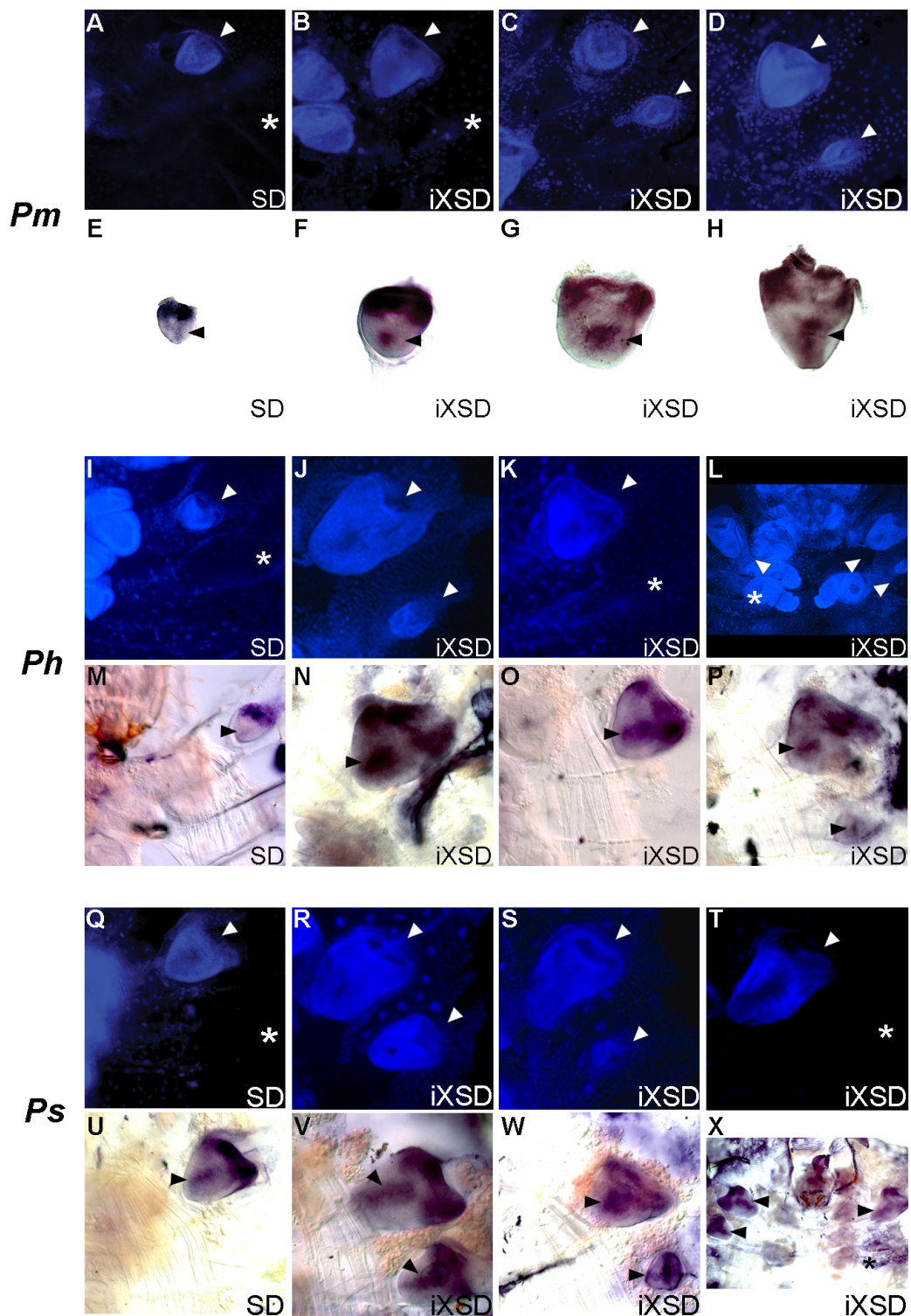
**Fig. S7.**



**Fig. S8. The relative size ranges of methoprene induced supersoldiers overlap with those of anomalous and naturally produced supersoldiers.** The x-axis shows the relative size range of supersoldiers as indicated by horizontal black bars, which was calculated in three steps: (i) the mean supersoldier (XSD)/soldier (SD) size ratio was taken by dividing the mean size (head width in mm) of either induced, anomalous, or evolved XSD adults or larvae by the mean size (head width in mm) of their respective normal SD adults or larvae; (ii) the maximum XSD/SD size ratio was calculated by dividing the largest induced, anomalous, or naturally produced XSD adult or larva in the sample by the mean size of their respective normal SD adults or larvae; and (iii) the minimum XSD/SD size ratio was calculated by dividing the smallest induced, anomalous, or naturally produced XSD adult or larva in the sample by the mean size of their respective normal SD adults or larvae. The vertical gray bar denotes the region of overlap between the relative size ranges of methoprene induced supersoldier adults and larvae and those of anomalous and naturally produced supersoldiers.

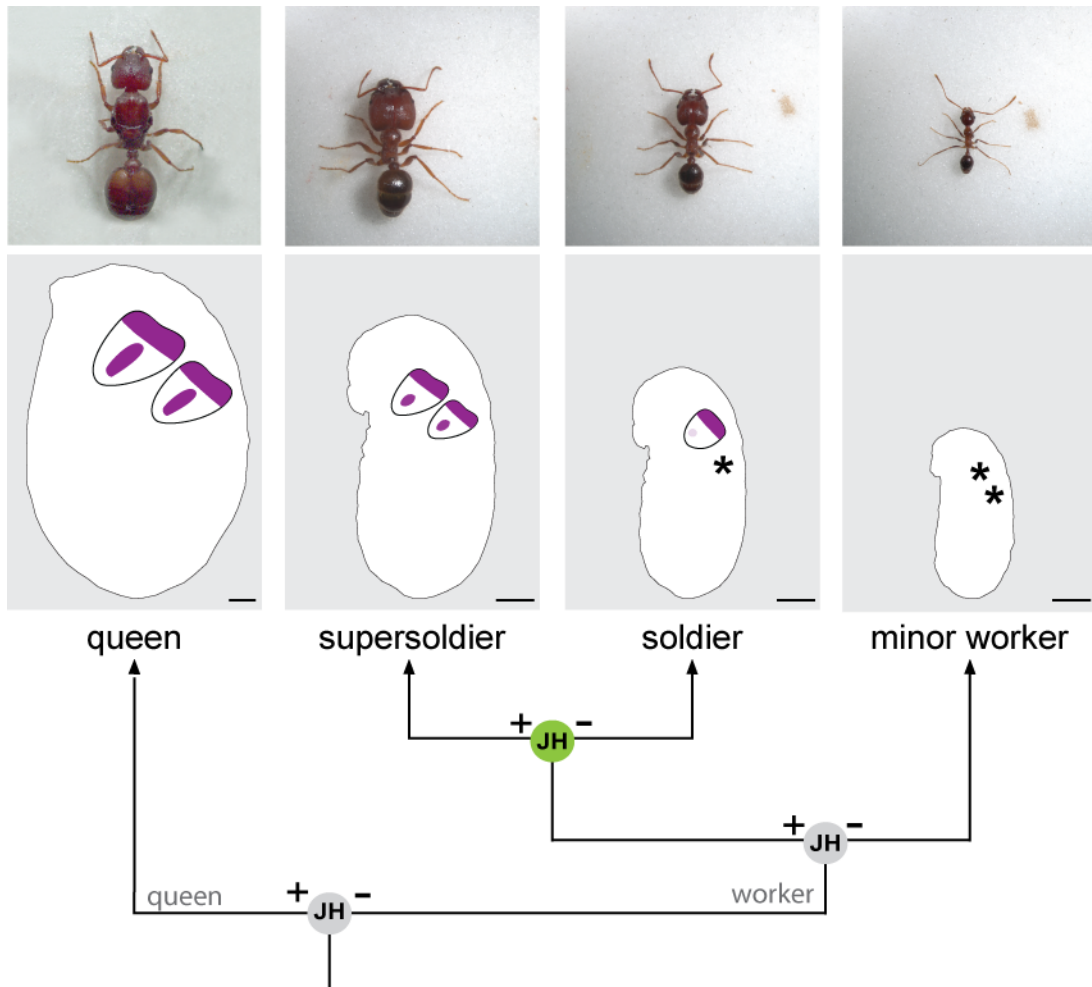
**Fig. S8.**

**Fig. S9. Variation in the number, size, and expression of *sal* in vestigial wing discs of normal soldier (SD) and induced supersoldier (iXSD) larvae in *P. morrisi* (Pm), *P. hyatti* (Ph), and *P. spadonia* (Ps).** (A to X), asterisks indicate absence of visible wing primordia, while white arrows indicate variation in the number of vestigial wing discs stained with DAPI. Black arrows indicate variation in wing pouch expression of *sal*. (A to X), images are to scale, with the exception of (L) and (X) that were taken at lower magnification to show asymmetry in the number of vestigial wing discs between the left and right sides of an induced supersoldier larva. Note that this induced variation in iXSD larvae is not due to the incomplete induction of JH, but rather is due to the release of hidden variation that has not yet been subject to selection. We detected variants (B and K and T) that we consider to be iXSD larvae, but which have only one pair of visible extra-large vestigial wing discs. This is because we define iXSD larvae by finding the smallest larva (shortest larval length in mm) in our sample that had two pairs of vestigial wing discs, and then considered any larva longer than this as iXSD larvae. That these are iXSD larvae rather than incompletely induced larvae is further supported by the existence of asymmetrical iXSD larvae: some iXSD have supersoldier-like vestigial fore- and hindwing discs on one side but only a forewing disc on the other side (L and X).

**Fig. S9.**

**Fig. S10. Actualization of supersoldiers in *P. obtusospinosa* through the re-evolution of a second JH-sensitive period that mediates the switch (green) between soldiers and supersoldiers.** See fig. S11 for data supporting this conclusion and fig. S12 for models that may explain the mechanisms through which this second switch point evolved. Scale bars indicate the relative size of queen, soldier, and minor worker larvae. All adult images are to scale. Purple represents *sal* expression, whereas asterisks indicate absence of visible wing primordia and *sal* expression.

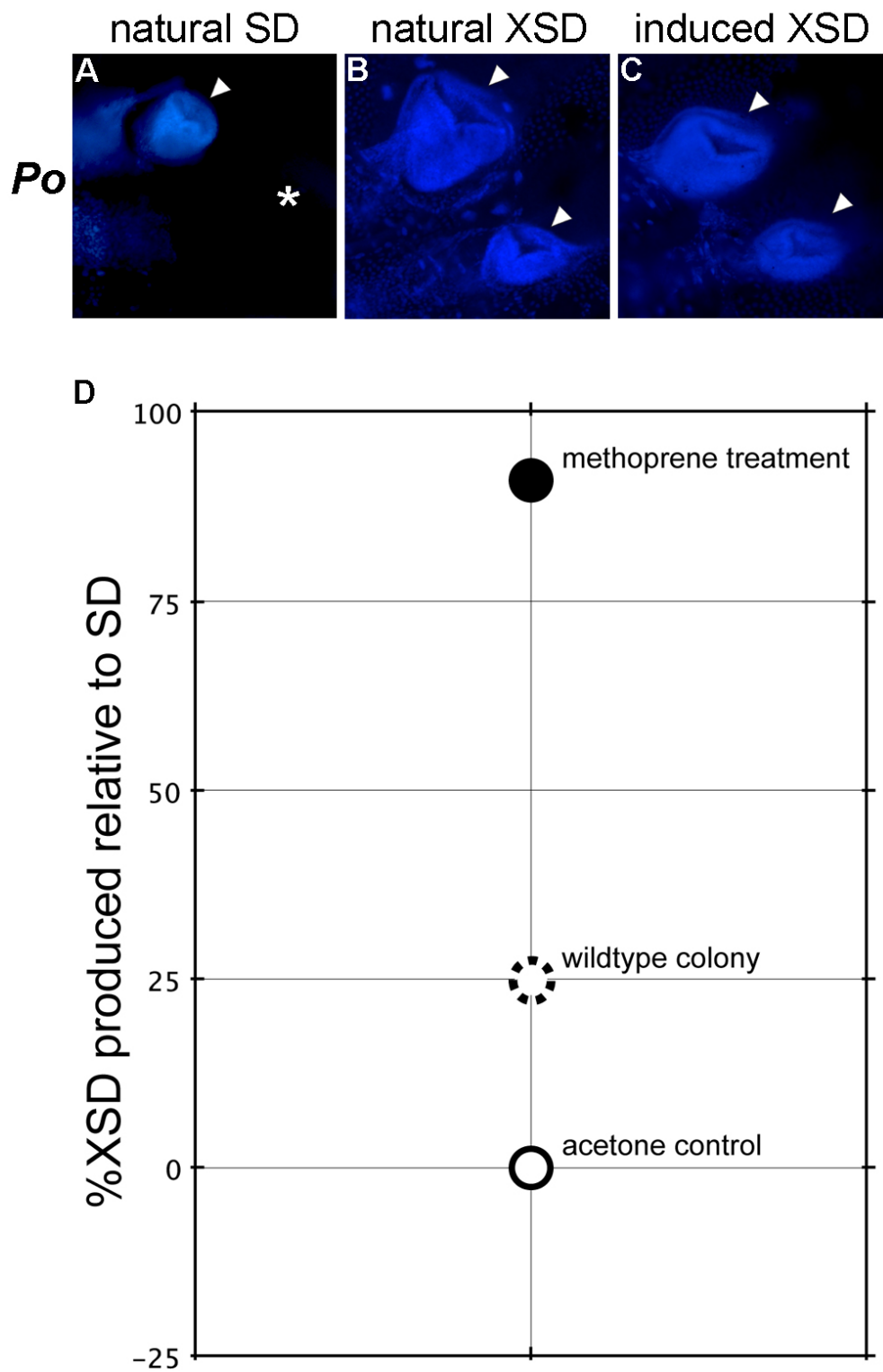
**Fig. S10.**



**Fig. S11. A second JH-sensitive period mediates the switch between the soldier and the supersoldier subcaste in *P. obtusospinosa*. (A to C)** All images are to scale.

Asterisks indicate absence of visible wing primordia, whereas white arrows indicate their presence. In *P. obtusospinosa* (*Po*), DAPI staining (blue) shows that, unlike (A) soldiers (SD) that have a single pair of vestigial forewing discs, (B) supersoldiers (XSD) and (C), methoprene-induced supersoldiers (iXSD) have two pairs of large vestigial wing discs. Furthermore, (D) y-axis shows the percent of XSD produced relative to SD in methoprene-treated larvae (black circle), acetone-treated control larvae (white circle), and in wild *P. obtusospinosa* colonies (12, 13) (dotted circle). A Fisher's exact test (one-tailed) shows that methoprene treatment produced a significantly greater proportion of XSD larvae than in acetone treated controls ( $P < 0.0001$ ). Methoprene treatment also produced a greater proportion of XSD larvae than that normally observed in wild colonies. This indicates that the development of SD and XSD subcastes in *P. obtusospinosa* are determined through a second JH-sensitive period that mediates the switch between SD and XSD. Methoprene- or acetone-treated larvae that did not develop into XSD went on to develop as either SD or minor workers.

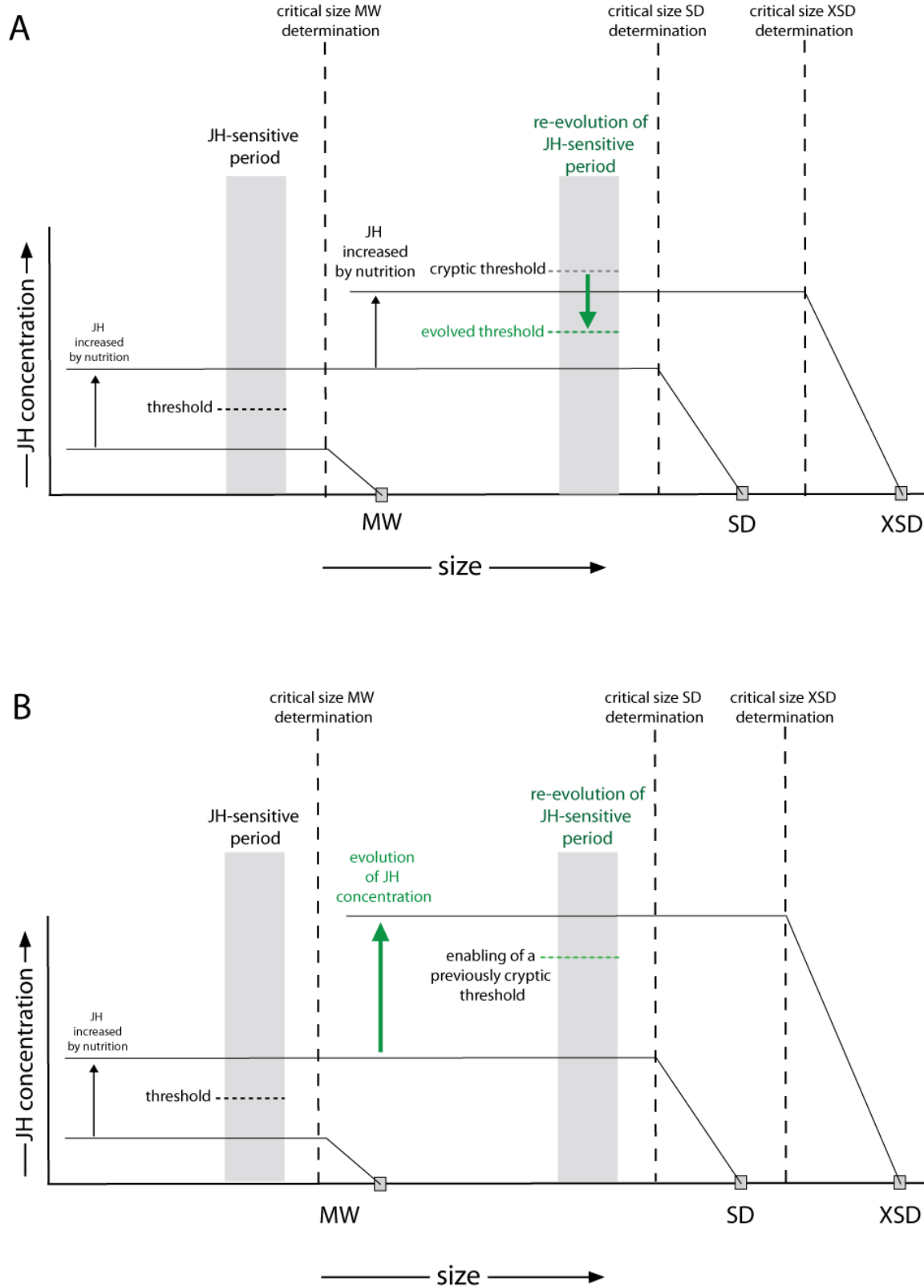
Fig. S11.



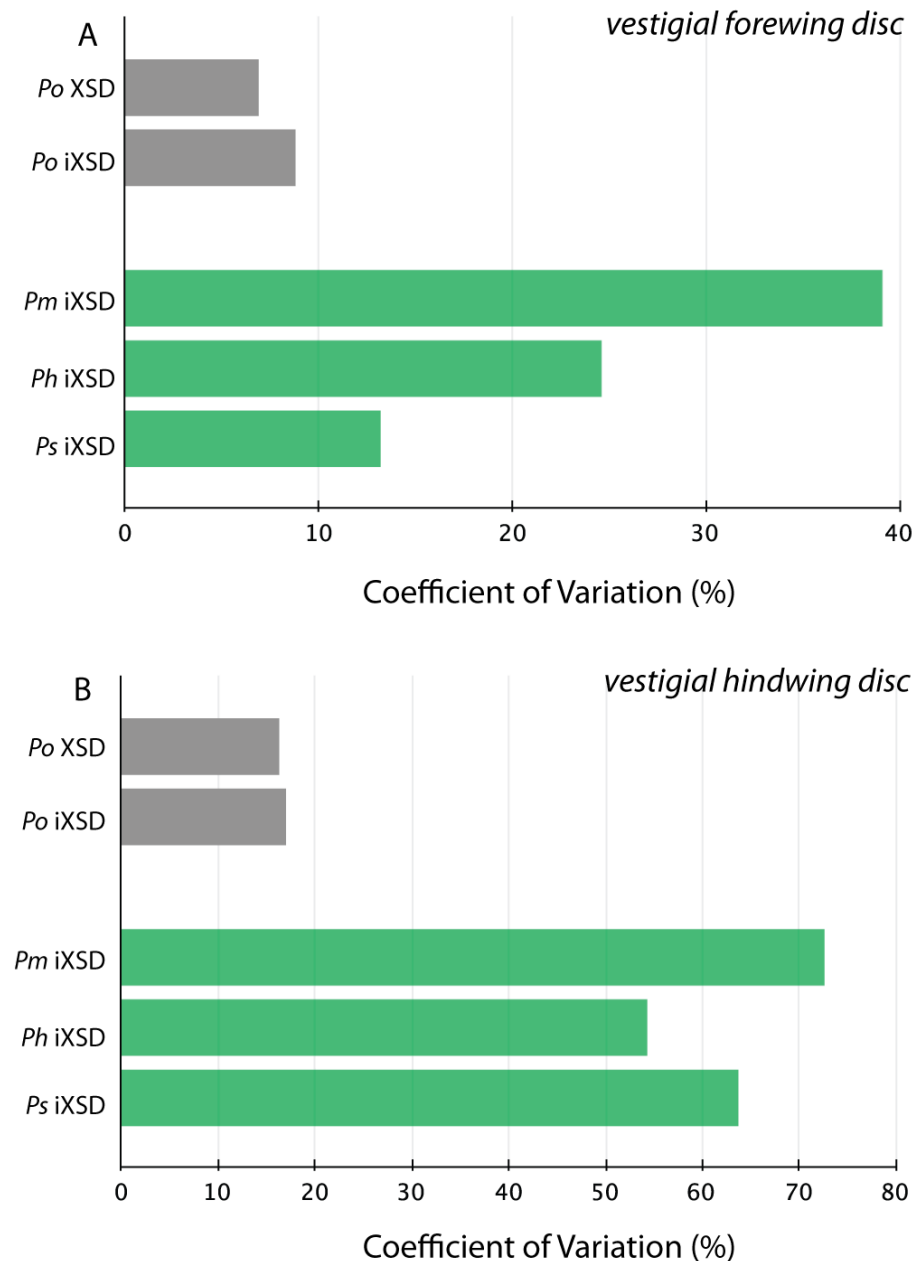
**Fig. S12. Two heuristic models showing how natural selection on the JH system may lead to the re-evolution of a continually produced supersoldier subcaste in *P.***

***obtusospinosa.*** The re-evolution of a supersoldier subcaste may have occurred either by a decrease in threshold sensitivity (as indicated by the green arrow in model **A**) or increase in JH level (as indicated by the green arrow in model **B**). In both models, the switch between minor workers (MW) and soldiers (SD), as well as between SD and supersoldiers (XSD), requires an intact JH-sensitive period. The JH-sensitive period is the period during which all of the key elements, including JH level and threshold, are present for the transduction of an environmental cue into a binary developmental decision (41). The threshold is made up of tissue responsiveness via a receptor complex, whereas JH level is determined by a balance of synthesis and degradation (42). Note that in both models the threshold and JH level is shown as static for simplicity – the threshold can be modulated, for example, by proportion of adult soldiers in the colony (43), whereas JH levels can be modulated, for example, in response to variation in environmental cues (41). In both models, if JH levels are below threshold during the JH-sensitive period, larvae initiate metamorphosis upon reaching the critical size for minor workers (16). If JH levels are above threshold, larvae continue to grow, their vestigial forewing imaginal discs appear, and the critical size is set (16). Metamorphosis at the soldier critical size is controlled by a sensitive period that precedes it (16). We propose that in the vast majority of *Pheidole* species there is a cryptic threshold that is set higher than the JH level, and therefore, all individuals initiate metamorphosis only at the soldier critical size (SD). In the case of anomalous supersoldier-like individuals, interaction between the ancestral developmental potential and induction by the environment causes the larva to

surpass this cryptic threshold by triggering the setting of a larger critical size (XSD). The re-evolution of supersoldiers in *P. obtusospinosa* involves the actualization of the induced ancestral developmental potential such that a regular proportion of larvae, which surpassed both the minor worker and soldier threshold, are determined to be supersoldiers. The actualization can be achieved by natural selection on an evolved decrease in threshold sensitivity in model **A** or by natural selection on an increase in JH level as in model **B**.

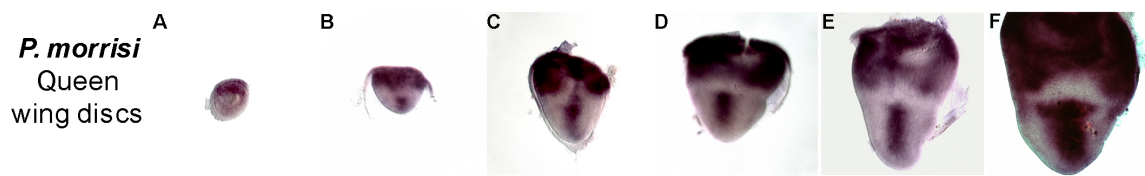
**Fig. S12.**

**Fig. S13. A signature of natural selection on the vestigial wing discs in naturally produced supersoldiers in *P. obtusospinosa*.** The naturally produced supersoldiers (XSD) and methoprene induced supersoldiers (iXSD) in *P. obtusospinosa* (*Po*) (fig. S11) generally show less variation in their size of (A) forewing and (B) hindwing vestigial discs than that of (A) forewing and (B) hindwing vestigial discs of the iXSD larvae of *P. morrisi* (*Pm*), *P. hyatti* (*Ph*), and *P. spadonia* (*Ps*), all of which lack a XSD subcaste. Furthermore, in *Pm*, *Ph*, and *Ps*, we also observed variation in the number of vestigial wing discs, asymmetry of vestigial wing discs as well as variation in the expression of *sal* (fig. S9). Greater variation is expected in an induced response that has not yet been subject to selection, which suggests that the developmental response of vestigial wing discs to JH has been canalized by selection in *P. obtusospinosa*, but not in *Pheidole* species that lack XSD.

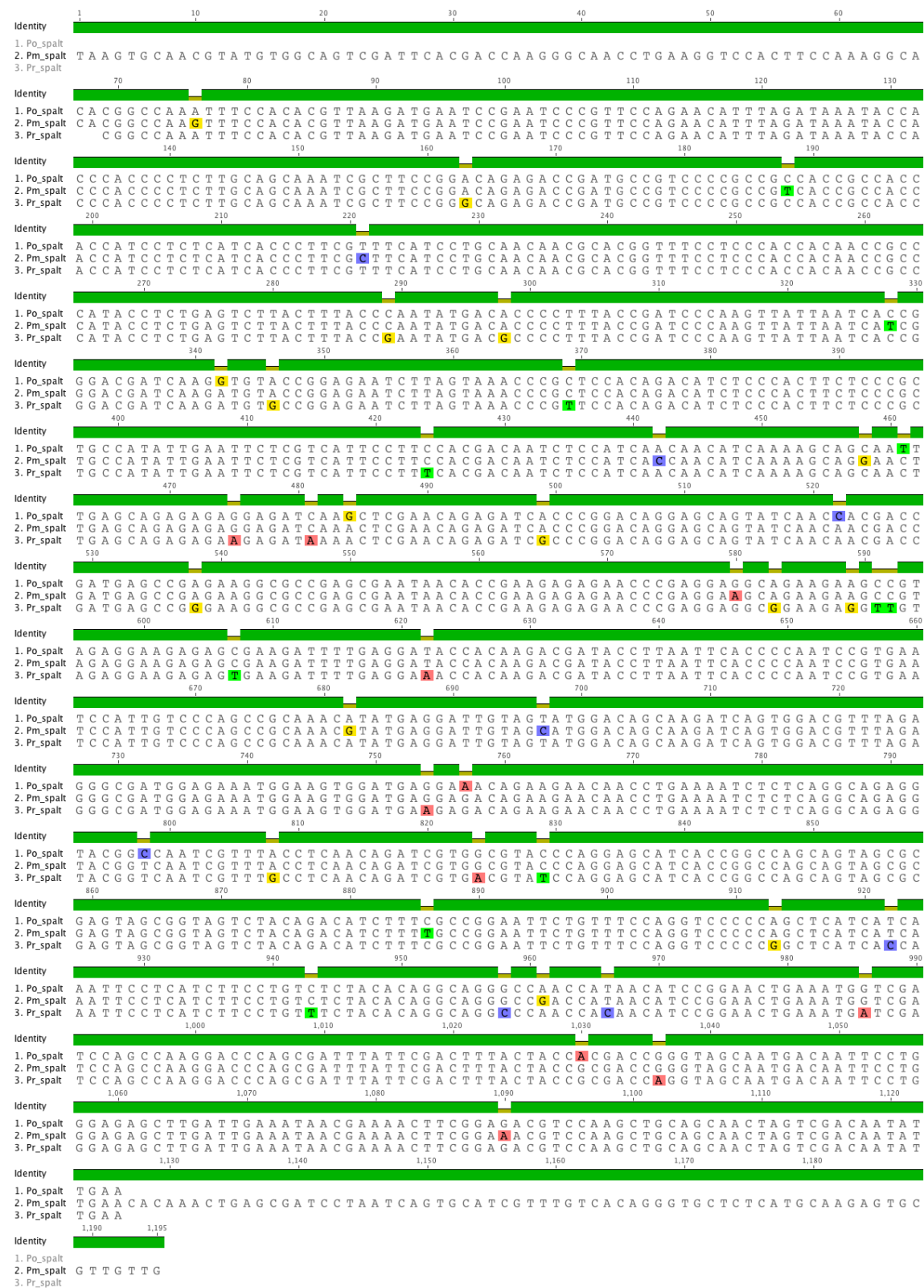
**Fig. S13.**

**Fig. S14. Dynamic expression of *sal* during wing disc development in *P. morrisi* queens suggests that the winglessness of adult supersoldiers (XSD) in *P. obtusospinosa* evolved through selection on environmentally induced supersoldier variants with novel interruption of *sal* expression.** (A to F) All images are to scale. The wing discs of queens appear and begin to grow early in development during the first larval instar. *sal* mRNA expression (purple) in these discs remains constant in the hinge, but is dynamic in the wing pouch where it increases in length as development of the disc progresses. In normal soldier (SD) forewing discs, interruption of *sal* expression (Fig. 1) is similar to (A) *sal* expression at the earliest stages of wing disc development in queens, which results in the development of completely wingless soldiers (Fig. 1). In contrast to normal SD, vestigial wing discs in methoprene induced supersoldiers (iXSD) are larger in size and their *sal* expression (fig. S9) is interrupted at a later time, similar to that of (B to D) queen wing disc development. These results, together with the fact that wing vestiges appear on the mesothorax of iXSD (Fig. 3C) and anomalous XSD adults (Fig. 2D), suggest that wing development has been reactivated in iXSD and anomalous XSD. Wing development, however, is not completed because unlike queen wing discs, SD wing discs only appear in last instar SD larvae and their growth is prematurely halted as they have to undergo metamorphosis sooner than queen wing discs. Collectively, these observations suggest that the evolution of wingless adult XSD in *P. obtusospinosa* (Fig. 2I) evolved through selection on environmentally induced supersoldier variants with a novel interruption of *sal* such that any maladaptive development of wings is completely halted.

**Fig. S14.**

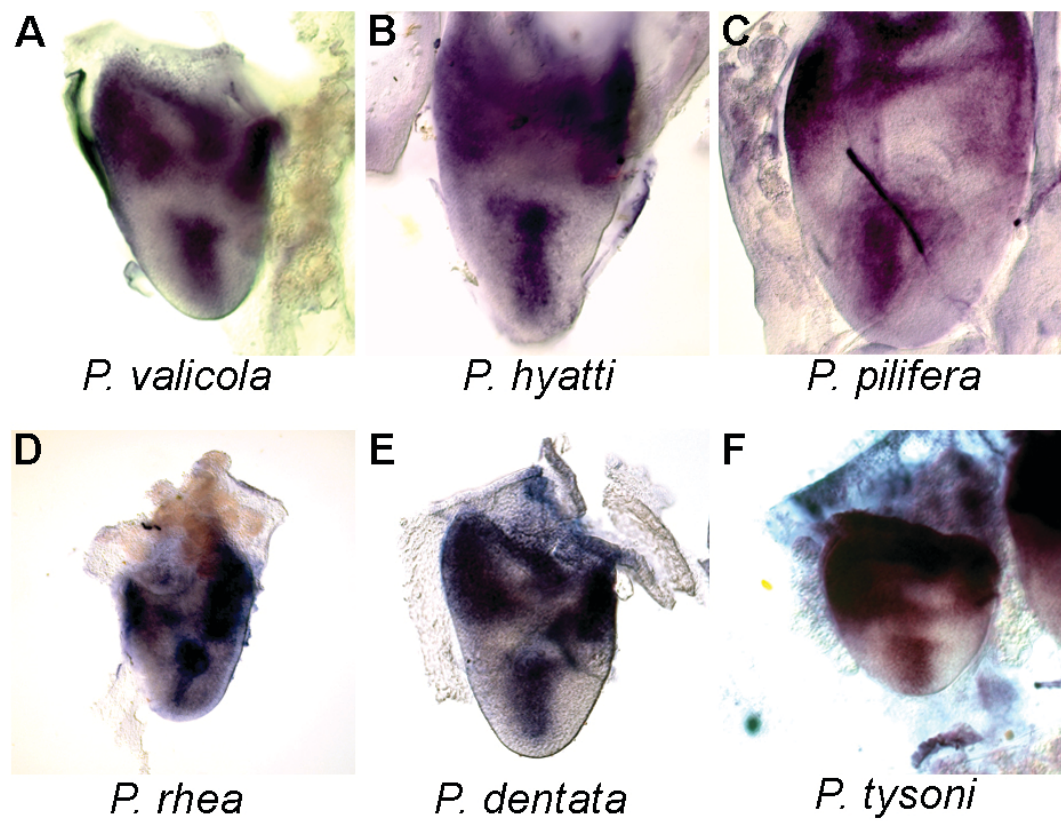


**Fig. S15. Sequence alignment of *sal* orthologs in *P. morrisi*, *P. rhea*, and *P. obtusospinosa* shows a 96% sequence similarity between their sequences.** Sequence identity (dark green bar) is indicated for each nucleotide position above sequence alignment. 1078 nucleotides are conserved between the sequences of all three species, and there are only 46 unique sequence differences, which are marked by different colors (unique changes to G are in yellow, C in purple, T in light green, A in red).

**Fig. S15.**

**Fig. S16.** *In situ* hybridization using a *P. morrisi* *sal* antisense probe detects a conserved expression pattern of *sal* in the wing discs of winged castes in six different *Pheidole* species. (A to F) *sal* mRNA expression (purple) in the wing discs of winged castes showing a conserved pattern of expression in the hinge and wing pouch (Fig. 1)(*I*) in both basal and derived *Pheidole* species (fig. S5).

**Fig. S16.**



## Supplementary Tables

**Table S1.** PCR primers used for genes in phylogenetic analysis of 11 *Pheidole* species.

Gene	Primer	Sequence	Reference
<i>cox1</i>	Forward: LCO1490	5'- GGTCAACAAATCATAAAGATATTGG - 3'	(44)
<i>cox1</i>	Reverse: HCO2198	5'- TAAACTTCAGGGTGACCAAAAAATCA - 3'	(44)
<i>cytb</i>	Forward: CB-J-10933	5'- TATGTAACACCATGAGGACAAATATC - 3'	(45)
<i>cytb</i>	Reverse: TS1-N-11683	5'- TATTCTTTATTATGTTTCAAAC - 3'	(45)
<i>lwr</i>	Forward: LR143F	5'- GACAAAGTKCCACCRGARATGCT - 3'	(46)
<i>lwr</i>	Reverse: LR639ER	5'- YTTACCGRTTCCATCCCRAACA - 3'	(46)

**Table S2. Genbank accession numbers for genes sequenced for phylogenetic analysis of 11 *Pheidole* species.**

Species	GenBank Accession # for mtDNA COxI	GenBank Accession # for mtDNA cyt b	GenBank Accession # for nDNA LW-Rh
<i>Pheidole megacephala</i>	JN205088	JN205099	JN205077
<i>Pheidole moerens</i>	JN205089	JN205100	JN205078
<i>Pheidole spadonia</i>	JN205090	JN205101	JN205079
<i>Pheidole tysoni</i>	JN205091	JN205102	JN205080
<i>Pheidole rhea</i>	JN205092	JN205103	JN205081
<i>Pheidole obtusospinosa</i>	JN205093	JN205104	JN205082
<i>Pheidole hyatti</i>	JN205094	JN205105	JN205083
<i>Pheidole vallicola</i>	JN205095	JN205106	JN205084
<i>Pheidole pilifera</i>	JN205096	JN205107	JN205085
<i>Pheidole morrisi</i>	JN205097	JN205108	JN205086
<i>Pheidole dentata</i>	JN205098	JN205109	JN205087

## SUPPLEMENTARY REFERENCES:

31. A. Bhatkar, W. H. Whitcomb, *Fla. Entomol.* **53**, 229 (1970).
32. N. H. Patel, *Methods Cell Biol.* **44**, 445 (1994).
33. D. Tautz, C. Pfeifle, *Chromosoma* **98**, 81 (1989).
34. F. Ronquist, J. P. Huelsenbeck, *Bioinformatics* **19**, 1572 (2003).
35. J. D. Thompson, T. J. Gibson, F. Plewniak, F. Jeanmougin, D. G. Higgins, *Nucleic Acids Res.* **24**, 4876 (1997).
36. W. P. Maddison, D. R. Maddison, MacClade: analysis of phylogeny and character evolution (Sinauer Associates, Sunderland, ver4.06, 2003).
37. D. Posada, K. A. Crandall, *Bioinformatics* **14**, 817 (1998).
38. D. Posada, T. R. Buckley, *Syst. Biol.* **53**, 793 (2004).
39. G. Ruxton, *Behav. Ecol.* **17**, 688 (2006).
40. R. R. Sokal, F. J. Rohlf, *Biometry*. (W.H. Freeman, New York, 1995).
41. H. F. Nijhout, *Bioscience* **49**, 181 (1999).
42. H. F. Nijhout, *Insect hormones*. (Princeton University Press, Princeton, 1994), pp. xi, 267 p.
43. D. E. Wheeler, H. F. Nijhout, *J. Insect Physiol.* **30**, 127 (1984).
44. O. Folmer, M. Black, W. Hoeh, R. Lutz, R. Vrijenhoek, *Mol. Mar. Biol. Biotechnol.* **3**, 294 (1994).
45. C. Simon *et al.*, *Ann. Entomol. Soc. Am.* **87**, 651 (1994).
46. P. S. Ward, D. A. Downie, *Syst. Entomol.* **30**, 310 (2005).